AGU PUBLICATIONS

Tectonics

RESEARCH ARTICLE
10.1002/2015TC003919

Key Points:
- A new approach using the 9D-space fault slip inversion method is presented
- The separation of stress states from heterogeneous data is performed
- Five successive tectonic episodes are detected

Supporting Information:
- Figure S1
- Figure S2
- Table S1

Correspondence to:
O. M. A. Radaideh,
o.sabbah@ymail.com

Citation:
Radaideh, O. M. A., and R. Melichar (2015), Tectonic paleostress fields in the southwestern part of Jordan: New insights from the fault slip data in the southeastern flank of the Dead Sea Fault Zone, *Tectonics*, *34*, 1863–1891, doi:10.1002/2015TC003919.

Received 1 MAY 2015
Accepted 14 AUG 2015
Accepted article online 18 AUG 2015
Published online 21 SEP 2015

Tectonic paleostress fields in the southwestern part of Jordan: New insights from the fault slip data in the southeastern flank of the Dead Sea Fault Zone

Omar M. A. Radaideh[1] and Rostislav Melichar[1]

[1]Department of Geological Sciences, Masaryk University, Brno, Czech Republic

Abstract A new approach for paleostress analysis, using the nine-dimensional space fault slip inversion method, was performed in the southeastern flank of the Jordan-Dead Sea Fault. Five major tectonic episodes with different kinematics were successfully detected from the inversion of a new fault slip data, which thereby caused reactivation of inherited crustal structures and established new ones. These episodes prevailed since Late Cretaceous times, and their chronological constraints were established essentially from the stratigraphic ages of the affected rocks and the crosscutting relationships of successive striae locally observed on the fault planes. During the Late Cretaceous to late Eocene, the area was under a compressional/strike-slip stress regime with a ~E-W trending σ_1. At Oligocene, a strike-slip stress regime with NW-SE striking σ_1 occurred. Both compression regimes correspond to the so-called Syrian Arc Deformation that gave rise to distinctive folds in Jordan and its surrounding areas. An extension with ~N-S to NE-SW trending σ_3 followed the late Oligocene compression event and took place during Miocene time, most probably linked to the opening of the Red Sea-Suez Rift. Late Cenozoic tectonics show the occurrence of two successive compressions, NW-SE then both NE-SW and ~N-S, which generally reflect a continental collisional setting between the Arabian and Eurasian plates.

1. Introduction

The Levant area, also known as the easternmost part of the Mediterranean Sea, lies within a complex tectonic zone of the interaction of three major lithospheric plates: Arabian, African, and Anatolian-Eurasian plates (Figure 1). The resulting deformation occurs along these plate boundaries [e.g., *Lyberis et al.*, 1992; *Mcclusky et al.*, 2000].

The area has tectonically evolved in a long time of deformation phases. The tectonic history started during late Palaeozoic-early Mesozoic time that led to the development of the Eastern Mediterranean basin and its associated passive margins, followed by a sequence of rifting and subsidence [e.g., *Ben-Avraham*, 1989; *Gardosh et al.*, 2008; *Garfunkel*, 1998; *Homberg and Bachmann*, 2010; *Robertson*, 1998]. Then, the convergence between Eurasia and Afro-Arabia occurred in the late Mesozoic [e.g., *Dilek and Rowland*, 1993; *Garfunkel*, 1998; *Sengor and Yilmaz*, 1981]. This convergence caused the initiation of the Alpine Orogen and a northward-dipping subduction zone in the areas of Cyprus and southern Turkey, as well as the ophiolite emplacement at several parts across the eastern Mediterranean region [*Dilek*, 2006; *Hawie*, 2014; *Parlak and Delaloye*, 1999; *Robertson*, 1998; *Sengor and Yilmaz*, 1981].

The progressive closure of the Neotethys and the coincident collision of the Eurasian and Afro-Arabian plates led to a horizontal compression of the whole Levant passive margin, resulting in the formation of a huge S-shaped fold belt at several places along the Levant area which is known as the Syrian Arc fold-thrust belts [e.g., *Eyal*, 1996; *Garfunkel*, 1998; *Kazmin*, 2002; *Walley*, 1998]. Northern Sinai, Israel, Palestine, Jordan, Lebanon, and Syria are crossed by a series of surface and subsurface anticlines and synclines that strike mostly in an ENE, NE, and NNE direction. The age of the Syrian Arc Deformation (SAD) is a subject of debate but is usually assigned from Turonian to Neogene [e.g., *Baer and Reches*, 1989; *Eyal and Reches*, 1983; *Joseph-Hai et al.*, 2010; *Shahar*, 1994; *Walley*, 1998].

Eyal [1996], who studied the trend and age of many structures throughout Israel and Sinai, suggested that the Syrian Arc Deformation in the Levant area may have continued up to the Quaternary times. The Cenozoic tectonic history of the eastern Mediterranean region experienced successive episodes of continental collision and breakup, resulting mainly in the formation of the Bitlis-Zagros suture zone, separating both the Arabian

plate and the Sinai subplate from the Afro-Arabian plate, opening the Red Sea, and developing the large-

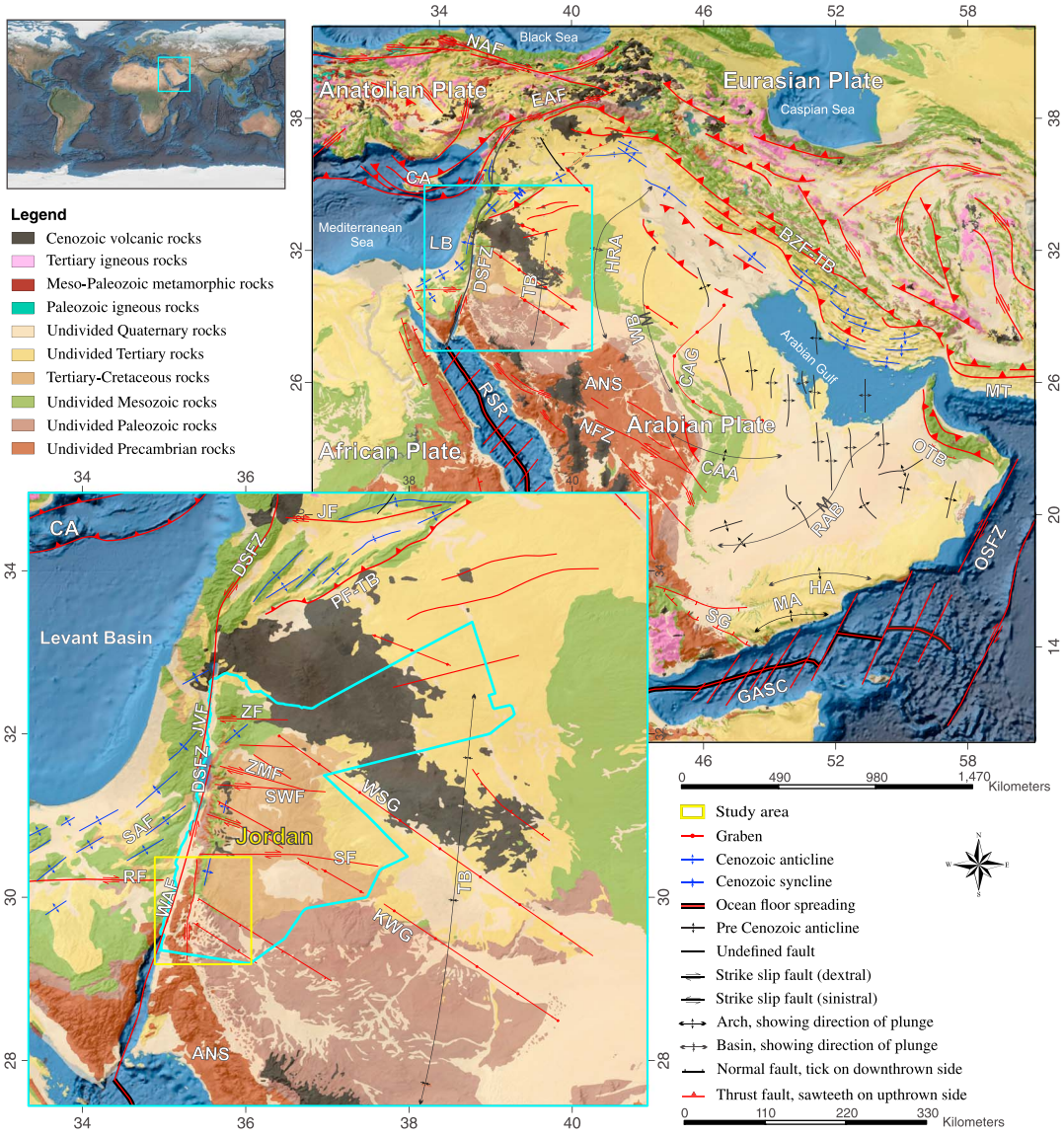

Figure 1. Generalized geological units and major tectonic elements of the Middle East region. The yellow square of the map indicates the study area discussed in this paper. Key to lettering: ANS, Arabian-Nubian Shield; BZF-TB, Bitlis-Zagros Fold and Thrust Belt; CA, Cyprian Arc; CAA, Central Arabian Arch; CAG, Central Arabian Graben; DSFZ, Dead Sea Fault Zone; EAF, East Anatolian Fault; GASC, Gulf Aden Spreading Center; HA, Hadhramout Arch; HRA, Ha'il-Rutbah Arch; JF, Jhar Fault; JVF, Jordan Valley Fault; KWG, Karak-Wadi Al Fayha Graben; LB, Levant Basin; MA, Mukalla Arch; MT, Makran Thrust; NAF, North Anatolian Fault; NFZ, Najd Fault Zone; OSFZ, Owen Sheba Fracture Zone; OTB, Oman Thrust Belt; PF-TB, Palmyra Folds and Thrust Belts; RAB, Rub Al Khali Basin; RF, Ramon Fault; RSR, Red Sea Rift; SAF, Syrian Arc Folds; SF, Salwan Fault; SG, Sadah Graben; SWF, Suwaqa Fault; TB, Tabuk Basin; WAF, Wadi Araba Fault; WB, Widyan Basin; WSG, Wadi Sirhan Graben; ZF, Zarqa Fault; ZMF, Zarqa-Ma'in Fault. The geological information of the Middle East area, provided by the U.S. Geological Survey Energy Resources Program (http://energy.usgs.gov/), superimposed on the global hillshading and Blue Marble images [*Becker et al.*, 2009; *Stockli et al.*, 2005]. The major tectonic elements of the Middle East area are compiled from *Alavi* [1991], *Beicip* [1981], *Brew* [2001], *Dilek* [2010], *Fox and Ahlbrandt* [2002], *McClusky et al.* [2000], *Taymaz et al.* [1991], and *Ziegler* [2001].

scale strike-slip faults, one of these is broadly known as the Dead Sea Fault Zone (DSFZ) [e.g., *Dilek*, 2006; *Garfunkel*, 1981, 1998; *Hempton*, 1987; *Lyberis et al.*, 1992; *Wdowinski and Zilberman*, 1997]. The Dead Sea Fault Zone (DSFZ) is an active plate boundary, connecting the Red Sea spreading system to the compressional deformation zones in the Bitlis-Zagros suture zone, and separating the Arabian plate from the Sinai-African plate [*Galli*, 1999; *Garfunkel*, 1981]. The Jordanian part of the DSFZ consists of two active segments: the Wadi Araba Fault (WAF) in the south and the Jordan Valley Fault (JVF) in the north.

Many geological studies were conducted in different countries of the Middle East in order to describe the tectonic evolution of the area. In spite of this, there are few paleostress studies for Jordan and its surrounding countries [e.g., *Aljumaily and Othman*, 2012; *Burdon*, 1959; *Diabat et al.*, 2004; *Eyal*, 1996; *Homberg et al.*, 2010; *Mikbel and Zacher*, 1981; *Zain-Eldeen et al.*, 2002; *Zanchi et al.*, 2002]. Two different models are used to explain the directions of paleostresses in the Levant area. One model considers two major stress field regimes that are responsible for the development of the identified tectonic structures [*Eyal and Reches*, 1983; *Eyal*, 1996]. The first regime, Late Cretaceous to Eocene, is characterized by E-W to WNW-ESE compression and attributed to the Syrian Arc stress field. The second regime, middle Miocene to recent, is characterized by N-S to NNW-SSE compression and is attributed to the Dead Sea stress field. The observations made in several studies [*Al-Khatib et al.*, 2010; *Atallah et al.*, 2002; *Diabat*, 2007, 2009; *Diabat et al.*, 2004] support this paleostress model. The other model shows more than two major paleostress field regimes [*Bahat et al.*, 2007; *Burdon*, 1959; *Hardy et al.*, 2010; *Letouzey and Tremolieres*, 1980; *Zain-Eldeen et al.*, 2002; and this study].

An extensive investigation of paleostress directions was conducted by *Letouzey and Tremolieres* [1980] in the northern part of the Arabian plate by analyzing a large number of tectonic stylolites, joints, shear planes, and faults. They identified four compression directions in both the northeastern and northwestern sides of the Arabian plate.

They related these directions to four deformation stages during Late Cretaceous, late Eocene-early Oligocene, late Miocene, and Plio-Quaternary. The recorded compression directions in the northeastern side of the Arabian plate are 135°, 175°, NNW-SSE to N-S, and 025°, respectively. The corresponding compression directions obtained in the northwestern side of the Arabian plate are 135°, 150°, ~E-W to NW-SE, and N-S, respectively. *Burdon* [1959] identified three directions of compression from the investigation of macrostructures (mostly folds) in Jordan: 285°, 322°, and 349°. He associated these directions with three deformation stages during the Late Cretaceous, late Oligocene-early Miocene, and Plio-Quaternary, respectively. *Mikbel and Zacher* [1981] identified a distinct direction of maximum horizontal compression (Shmax) at 295° from analysis of the direction of many ruptures that effect on the Cretaceous strata in the monoclinal structure from Wadi Shueib, west of Jordan. *Salameh and Zacher* [1982] investigated horizontal stylolites in Jordan and reported Shmax at 315° and 350° for late Oligocene-early Miocene and Plio-Quaternary, respectively.

The first paleostress analysis obtained from fault slip data along the southeastern margins of the DSFZ (southwest of Jordan) was conducted by *Zain-Eldeen et al.* [2002]. Their results show a succession of seven brittle tectonic regimes from Neoproterozoic to Pleistocene times. Their results also show a general clockwise rotation with time of the Shmax from an E-W trend in the Cretaceous to N-S trend in the Pleistocene. They found the directions of the Shmax changed from E-W, NW-SE, NW-SE to NNW-SSE, and N-S, which approximately coincide with the Late Cretaceous, Eocene, Miocene, and late Pleistocene, respectively. *Hardy et al.* [2010] recognized five major tectonic events from the investigation of new structural data in Israel, comprising the following: early Mesozoic NE-SW oriented extension, Campanian NNE-SSW to NE-SW oriented extension, Paleocene WNW-ESE to NW-SE oriented compression, Eocene ~N-S oriented extension, and a complex late Cenozoic stress field. The late Cenozoic tectonic events are characterized by two major compressions, respectively trending NNW-SSE and WNW-ESE, a minor compression trending NE-SW, and two extensions striking NE-SW and E-W.

Determination of the paleostress tensors is an important tool to characterize successive tectonic episodes in deformed rocks and has been the object of detailed studies [e.g., *Delvaux et al.*, 1997; *Huibregtse et al.*, 1998; *Kaymakci et al.*, 2003; *Matzenauer*, 2012; *Pêcher et al.*, 2008; *Saintot and Angelier*, 2000, 2002; *Sippel et al.*, 2009].

Several techniques have been developed to determine paleostress tensors based on signs of brittle deformation noticeable in the field and described elsewhere in detail [e.g., *Angelier*, 1979, 1989, 1990; *Delvaux and Sperner*, 2003; *Yamaji*, 2000]. A new approach for the inversion of stress states, using the multiple inverse method [*Yamaji*, 2000] in nine-dimensional space [*Melichar and Kernstockova*, 2010], was applied here. In this approach, the paleostress tensors have been reconstructed based on a new fault slip data measured from the east flank of the Wadi Araba Fault (WAF), southern segment of the DSFZ, where excellent outcrops of Precambrian to Pleistocene rocks are available.

The aim of this study is to improve the knowledge of the paleostress patterns in the southwestern part of Jordan based on fault slip data analysis. The main tectonic elements of the Middle East and the location of the study area are shown in Figure 1.

2. Geological Setting

Jordan lies on the northern edge of the Arabian-Nubian Shield (ANS). The ANS is a part of the East African (Pan-African) Orogen (900 to 500 Ma) which is composed of a voluminous addition of Neoproterozoic juvenile crust derived from the accretion of oceanic and back arcs [e.g., *Duyverman et al.*, 1982; *Genna et al.*, 2002; *Küster*, 2009; *Stern*, 1994; *Stoeser and Frost*, 2006; *Vail*, 1983]. The ANS is locally exposed in the southwestern part of Jordan and represents the oldest rocks to be found in the area, predominantly of late Proterozoic. These rocks include various igneous and metamorphic suites, and are subdivided locally into two complexes, the older Aqaba and the younger Araba, with a regional unconformity (Saramuj conglomerate) between them [*Ibrahim and McCourt*, 1995; *Jarrar et al.*, 2003; *Rabb'a*, 1994; *Rashdan*, 1988].

An incomplete Paleozoic clastic succession above an angular Pre-Saq unconformity [*Sharland et al.*, 2001] is overlain the Proterozoic Arabian-Nubian Shield [*Bender*, 1975; *Powell*, 1989a; *Segev*, 1984]. The Paleozoic strata of southern Jordan comprise one of the most voluminous bodies of sediments in the region and consist of the Cambrian to Lower Ordovician Ram Group and the Ordovician to Silurian Khreim Group [*Powell*, 1989a]. The Ram Group, predominantly of pure, massive, and voluminous cross-bedded fluvial quartzarenites and arkose, was deposited in large braided alluvial systems on a very gentle slope under a humid climate [*Kolodner et al.*, 2006; *Powell*, 1989a].

Following that, a major marine transgression took place during the Lower Ordovician and deposited mature siliclastics of Khreim Group, predominantly cycles of fine to medium-grained quartzarenite and micaceous siltstone with mudstone [*Powell*, 1989a]. The effects of tectonic and global eustatic changes on the late Paleozoic and early Mesozoic sedimentation are evident by substantial gaps in the sedimentary records in the Paleozoic, Early Jurassic, and Early Cretaceous successions [*Gardosh et al.*, 2008]. Accordingly, an incomplete and spatially variable lower Paleozoic section across Jordan attributes to three phases of tilting, uplift, and erosion, which occurred in pre-Carboniferous, pre-Triassic, and pre-Cretaceous times [*Powell*, 1989a].

In the south Jordan, however, Devonian to Jurassic strata are missing, and Lower Cretaceous uncomfortably overlies sediments of lower Paleozoic ages [*Bender*, 1975; *Powell*, 1989b]. Three major mega-sequences (Kurnub, Ajlun, and Belqa groups) are recognized within the Cretaceous to Eocene succession in south Jordan. These sequences are generally characterized by passive continental margin depositional environments, which pass upward from alluvial/paralic to carbonate shelf and pelagic ramp settings [*Powell and Moh'd*, 2011]. The Lower Cretaceous Kurnub group was deposited in alluvial environments, which show an upward trend from a braided, low to high sinuosity alluvial plain. It composes mainly of the massive white to reddish, medium to coarse-grained sandstones [*Bender*, 1975; *Powell and Moh'd*, 2011]. The second mega-sequence comprises Cenomanian to Upper Coniacian carbonates and is characterized by a rapid rise in relative sea level with a depositional environment of rimmed carbonate shelf to hemi-pelagic/pelagic ramp. The upper Coniacian to late Eocene Belqa group represents the last marine phase which is composed mainly of chalk, chert, and phosphorite sediments, deposited in a pelagic or hemi-pelagic ramp setting. During late Eocene time, a regression of the Tethys Sea occurred and left widespread deposits of nummulitic carbonate rocks [*Powell*, 1989b; *Powell and Moh'd*, 2011]. Quaternary deposits are mostly of lacustrine sediments, fluviatile sand, gravel, and conglomerate, indicating continuous uplift movements and retreat of marine environment [*Bender*, 1975].

Structurally, the southwestern part of Jordan is generally framed by two major fault trends as inferred from mapping and field studies. One set trends N to NNE, which is mainly left-lateral strike-slip faults, such as the Wadi Araba and Al Quwayra faults. The other set trends NW, which is mainly normal faults, such as the Ras en Naqab- Batn Al Ghoul escarpments, and Dubaydib graben. The general structural and surficial geology of the southwestern corner of Jordan is shown in Figure 2.

3. Data and Paleostress Reconstruction

3.1. Fault Slip Data Collection

A total of 2266 mesoscale faults have been measured from 51 sites of different lithologies, spanning in age from the late Proterozoic to the Pleistocene (Figure 2). Most of investigated sites correspond to fresh outcrops along road cuts and active or abandoned quarries. A variety of fault strikes has been recorded with NNW-SSE to N-S and NE-SW trending maxima.

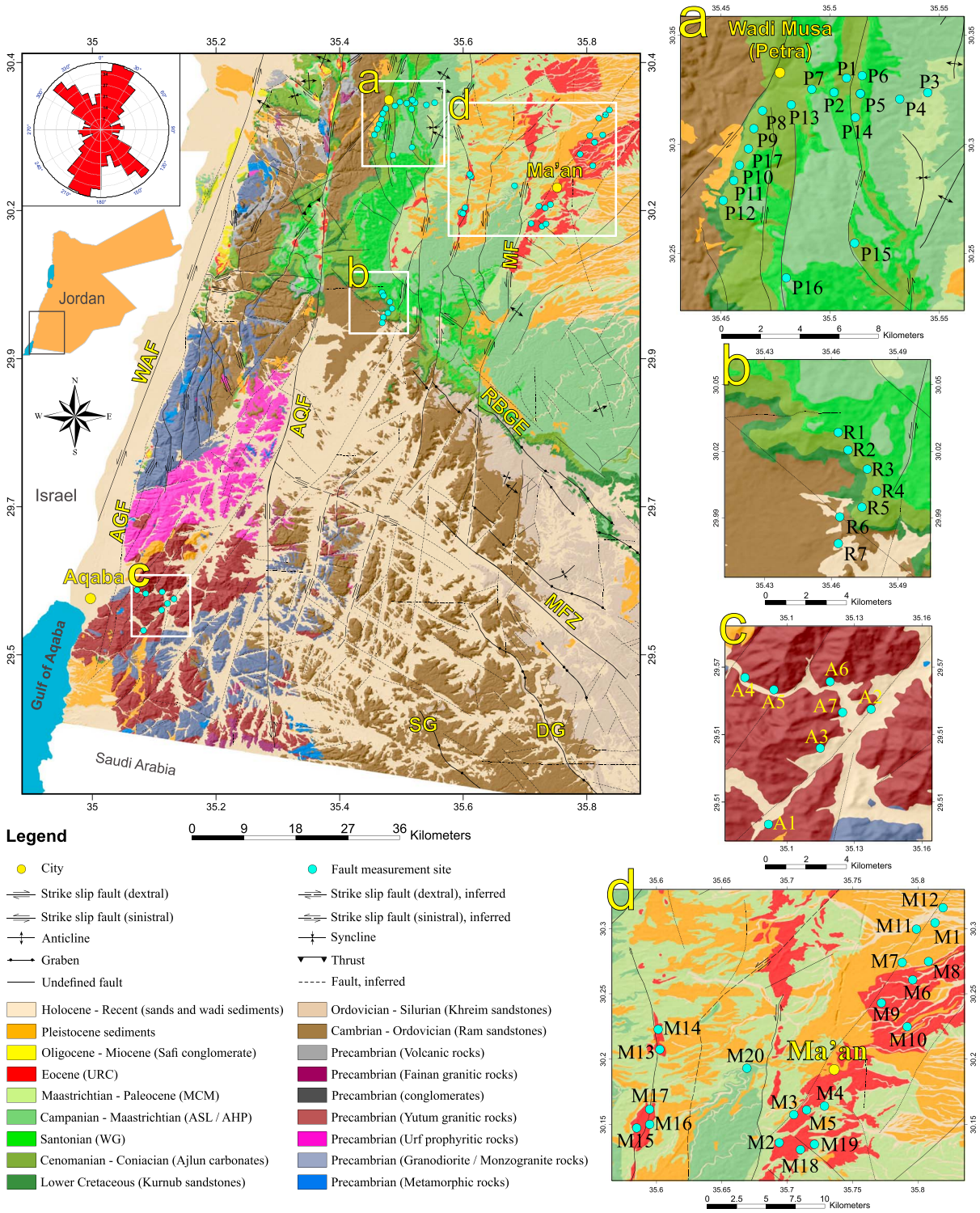

Figure 2. Generalized structural and geological map of the southwestern part of Jordan. The geological information which provided by the Jordanian Ministry of Energy and Mineral Resources (http://www.memr.gov.jo/), superimposed on a shaded digital elevation model (horizontal resolution 30 m). Rose diagram (inset) illustrates the strike directions of all structural features which were digitized with ArcGIS v10 from a 1:50,000 scale geological map of the southwestern part of Jordan. The locations of the fault slip measurement sites are shown. The following abbreviations are used: AGF, Aqaba-Gharandal Fault; AHP, Al Hisa Phosphorite Formation; AQF, Al Quwayra Fault; ASL, Amman Silicified Limestone Formation; DG, Dubaydib Graben; MCM, Muwaqqar Chalk Marl Formation; MF, Ma'an Fault; MFZ, Mudawwara Fault Zone; RBGE, Ras en Naqab-Batn Al Ghoul Escarpments; SG, Saladih Graben; URC, Umm Rijam Chert Limestone Formation; WAF, Wadi Araba Fault; WG, Wadi Umm Ghudran Formation.

Most of the measured faults are generally characterized by moderate to very steep inclined planes that bear horizontal to subhorizontal plunging striations. The datum for each mesoscale fault consists of dip and dip direction of fault plane, the azimuth and plunge of striation on the fault plane, and the sense of movement. The sense of slip on fault planes was determined from kinematic indicators such as accretionary mineral steps (mostly calcite and quartz), slickolites, riedel shear, and asymmetric elevations, among others. The typical kinematic indicators for shear sense determination were discussed in detail elsewhere [e.g., *Doblas*, 1998; *Lee*, 1991; *Petit*, 1987]. The failure to recognize the sense criteria, like in the case of the riedel shear criterion, has severe effects on stress calculations and may lead to misinterpretation of the faulting events even if the stress calculations are mathematically correct [*Hippolyte et al.*, 2012; *Sperner et al.*, 1993]. Wherever available, the determination of shear sense was usually performed from multiple sense criteria on the same plane to verify the consistency of shear sense. The mesoscale-exposed faults with ambiguous slip sense are not useful for the analysis [*Sperner and Zweigel*, 2010]. Overprinting relationships of fault striations though rare in the present study area (Figure 3) can be carefully used together with the age of host rocks as chronological indicators. However, the relative chronological indicators are not always obvious, which can lead to false interpretations of the tectonic events [e.g., *Hippolyte et al.*, 2012].

3.2. Stress Tensor Determination

Inversion of a fault slip data set in terms of paleostress reconstruction is based on the Wallace and Bott hypothesis [*Wallace*, 1951; *Bott*, 1959], stating that fault slip occurs parallel to the direction of the maximum shear stress. The fault slip data are inverted to determine four parameters of the reduced stress tensor: the orientations of three orthogonal principal stress axes σ_1, σ_2, and σ_3 (where $\sigma_1 \geq \sigma_2 \geq \sigma_3$), and the ratio of the principal stress differences ($\varphi = \sigma_2 - \sigma_3 / \sigma_1 - \sigma_3$).

The variation in stress fields may lead to newly formed faults or the reactivation of older ones. Generally, fault systems that have been generated or reactivated under more than one stress fields are commonly called heterogeneous. The heterogeneity characteristics of fault slip data set come also from the rock mass properties in which is undergoing the state of stress changes. Thus, the heterogeneous data sets are much more common in nature than homogeneous ones [e.g., *Angelier*, 1989; *Nemcok and Lisle*, 1995; *Yamaji et al.*, 2011]. Any attempt to calculate stress with heterogeneous fault slip data will result in a composite stress state which is a compromise between the actual stress states corresponding to several superimposed tectonic episodes [e.g., *Nemcok and Lisle*, 1995]. Therefore, it is important to strictly separate heterogeneous data into homogeneous subsets prior to the stress calculation. A common problem in paleostress analysis is to separate stress tensors from such a mixed data set [e.g., *Sperner and Zweigel*, 2010]. Several methods have been especially proposed for separating stresses from heterogeneous fault slip data, described in detail elsewhere [e.g., *Etchecopar et al.*, 1981; *Hansen et al.*, 2014; *Nemcok and Lisle*, 1995; *Nemcok et al.*, 1999; *Otsubo et al.*, 2006; *Shan et al.*, 2004; *Yamaji*, 2000; *Yamaji et al.*, 2006; *Žalohar and Vrabec*, 2007]. The separation procedures are generally based on both mechanical and kinematical compatibility and relative tectonic chronology data [*Lacombe*, 2012], but it is not always carefully made [e.g., *Lacombe*, 2012; *Sperner and Zweigel*, 2010].

New method was used for dealing with these heterogeneous data sets, and even homogeneous ones as well, and estimating possible stress states without previous separation into homogeneous subsets. The method is described by *Kernstocková and Melichar* [2009], which is based on the Wallace-Bott hypothesis. The processed fault slip data were expressed as unit vectors in 9D space using a noncommercial computer program "MARK2010" [*Kernstocková and Melichar*, 2009]. The program uses the multiple inverse procedures developed by *Yamaji* [2000]. The program has two new parameters that allow a detailed analysis of the reliability of the stress tensor solutions, comprising the stability criterion to control error-prone solutions caused by defective fault slip data and the reactibility criterion to distinguish solutions numerically correct but practically impossible. The main advantages of this method are that the data separation is a fully automatic and unbiased tool to select homogeneous subsets, as well as its applicability for faults that have been activated under several episodes of tectonic deformation, where the affiliation to unique fault generations is not clear. In particular, heterogeneous fault slip data set is separated into mechanically homogeneous subsets according to misfit angle between c-line and line of sigma-tensor in 9D (≈ cosine of this angle) and kinematic compatibility (sense of movement).

Using artificial homogeneous and heterogeneous fault slip data sets, we compared and verified this method with several different numerical techniques (e.g., the Right Dihedra, the Numerical Dynamic Analysis, and the P-T methods) that included the Win-Tensor [*Delvaux*, 2012], Tectonics FP [*Reiter and Acs*, 2000], T-Tecto

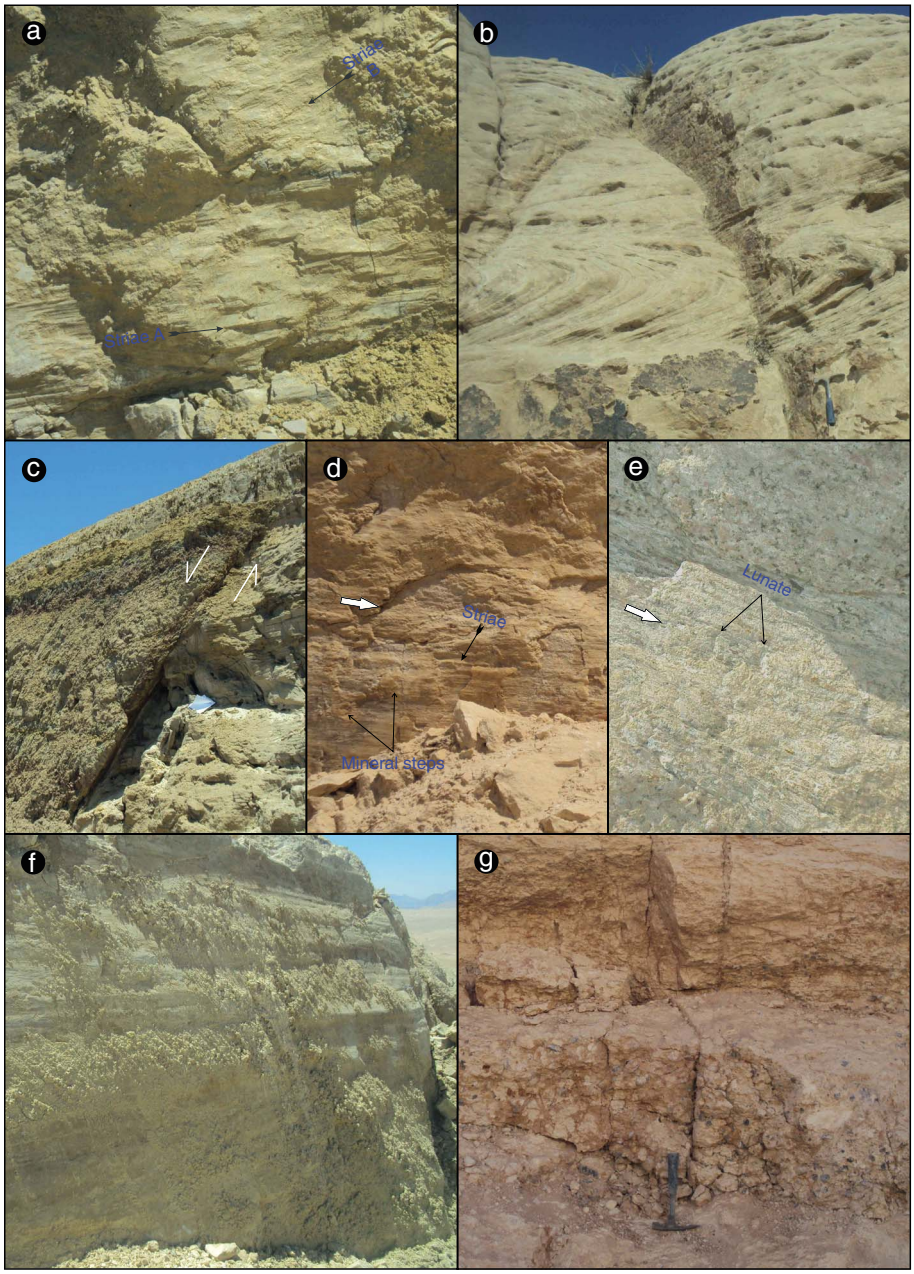

Figure 3. Examples of brittle structures observed in the field area. (a) Fault surface covered by two superimposed sets of striae. (b) Cross lamination in the lower Paleozoic sandstone. (c) Steeply dipping normal fault in the Upper Cretaceous strata exposed at site R2. (d) Fault plane showing sinistral strike-slip movement as observed from the calcite accretion steps. The white arrow indicates the direction of the share movement. (e) Fault plane showing normal slip movement as indicated from the crescentic fractures. (f) Large sinistral strike-slip fault with very pronounced striae cuts the Cenomanian Na'ur limestone formation at site R5. (g) Stratigraphic evidence of Quaternary faulting at site M9.

[*Žalohar*, 2009; *Žalohar and Vrabec*, 2007], and MIM Package [*Yamaji*, 2000; *Yamaji et al.*, 2005] computer programs (Figure S1 of the supporting information). A considerable consistency was generally found between the results of the present method and those of different inversion techniques considered [*Radaideh and Melichar*, 2014].

However, the current method resides in combining the fault slip data into four-element groups and calculating the reduced stress tensor for each group separately [*Melichar and Kernstockova*, 2010]. The four-fault

groups thus can be either homogeneous ones (i.e., four-fault groups of the same generation) or heterogeneous ones (i.e., four-fault groups of different generations). The calculations of the reduced stress for the heterogeneous groups are spurious and therefore appear scattered in the 9D space, whereas the calculations for the homogeneous groups appear in clusters and may represent true tectonic phases [*Kernstocková and Melichar*, 2009]. Watson density function [*Fisher et al.*, 1987] expanded to 9D space can be used to identify these clusters and to indicate the possible directions of considered principal stress. The number of such clusters indicates a minimal number of stress solutions. The calculated stress solutions are graphically shown both in the form of density maxima of the stress solutions for each principal stress (σ_1, σ_2, and σ_3) projected onto lower hemisphere equal-area plots and with prominent color-coded symbols of the respective principal stresses obtained from the 9D analysis. Once the stress solution is determined, the program calculates the misfit angels between the theoretical slip directions and measured ones for a given fault slip data.

3.3. Procedure of Analysis

The quality and reliability of paleostress analysis mainly depend first on the accuracy of field measurements. The consequences of the measurement inaccuracies will have direct effects on the precision of the stress calculations [e.g., *Hippolyte et al.*, 2012; *Sperner and Zweigel*, 2010]. For this reason, the preliminary measurement sets from each location were first checked by using the Mark program to ensure if the striae lie correctly on their respective fault planes. Fault slip data that were found with small deviations were corrected or orthogonalized so that striations and fault planes are precisely parallel; those data with large deviations ($>10°$) were excluded. This correction thus segregated about 13% of the total data sets which were not used in the next stage.

After having checked the data of each outcrop, the inversion procedure was then run on a complete data set of each location separately. The obtained stress states are visualized on the stereograms and represented by clusters of symbols that agree in terms of the directions of principal axes as well as the stress ratio, φ. The number of such clusters indicates a minimal number of stress solutions for a given set of fault slip data. The more precisely determined stress solutions were finally calculated using 9D density distribution function and were integrated in the density distribution plots. The resulting stress solutions consist of a stress configuration with the most relevant faults having misfit angle; the angle between measured and theoretical slip direction does not exceed 10°. For a comparative view, the stress separation process and the results as well were checked for consistency by applying the Multiple Inverse Method [*Yamaji*, 2000] through the MIM software. A significant degree of agreement was found between the results obtained by using both methods (Figure S2).

Most of the analyzed sites in the southwestern part of Jordan display evidence of polyphase faulting, which is indicated by differently oriented clusters of stress axes. Here is an example showing the numerical separation of heterogeneous fault slip data (Figure 4). By applying the multiple inverse method in 9D space (Mark program) to the measurements collected from site R1 (Figure 4a), three deformation regimes were determined: (1) an extension regime with an ~E-W striking σ_3, (2) a reverse regime with a NNW-SSE striking σ_1, and (3) a strike-slip regime with a NNW-SSE trending σ_1. On the other hand, the measurements collected from site P13 are only explained by a main stage of deformation corresponding to a strike-slip regime with computed σ_1 trending NE-SW (Figure 4b).

The local detected stress states at different sites were finally clubbed into coherent categories based on consistency of principal stress axis orientations rather than by the value of the stress ratio [e.g., *Saintot et al.*, 2011; *Tripathy and Saha*, 2013], as the latter is highly sensitive and may differ considerably with a limited range of fault orientations [*Lacombe*, 2012]. The separation of the results into coherent categories may have a number of adverse effects on the determination of stress ratio (φ), such as having a transpressional or transtensional regime. This is due to the separation that might split a population of results with a distribution of φ centered on 1 (in the case of transtension) or on 0 (in the case of transpression), into two almost symmetrical parts, with φ distributed around 0.75 in the first case and 0.25 in the second case. This therefore will lead to generate partial populations with apparent results and to multiply the number of apparent stress tensors. Among other things, it is almost impossible for such separation to get stress tensors with an exact mean φ value of 1.0 or 0.0, while this is absolutely possible in reality. This separation therefore also leads to a bias in the estimate of the φ values.

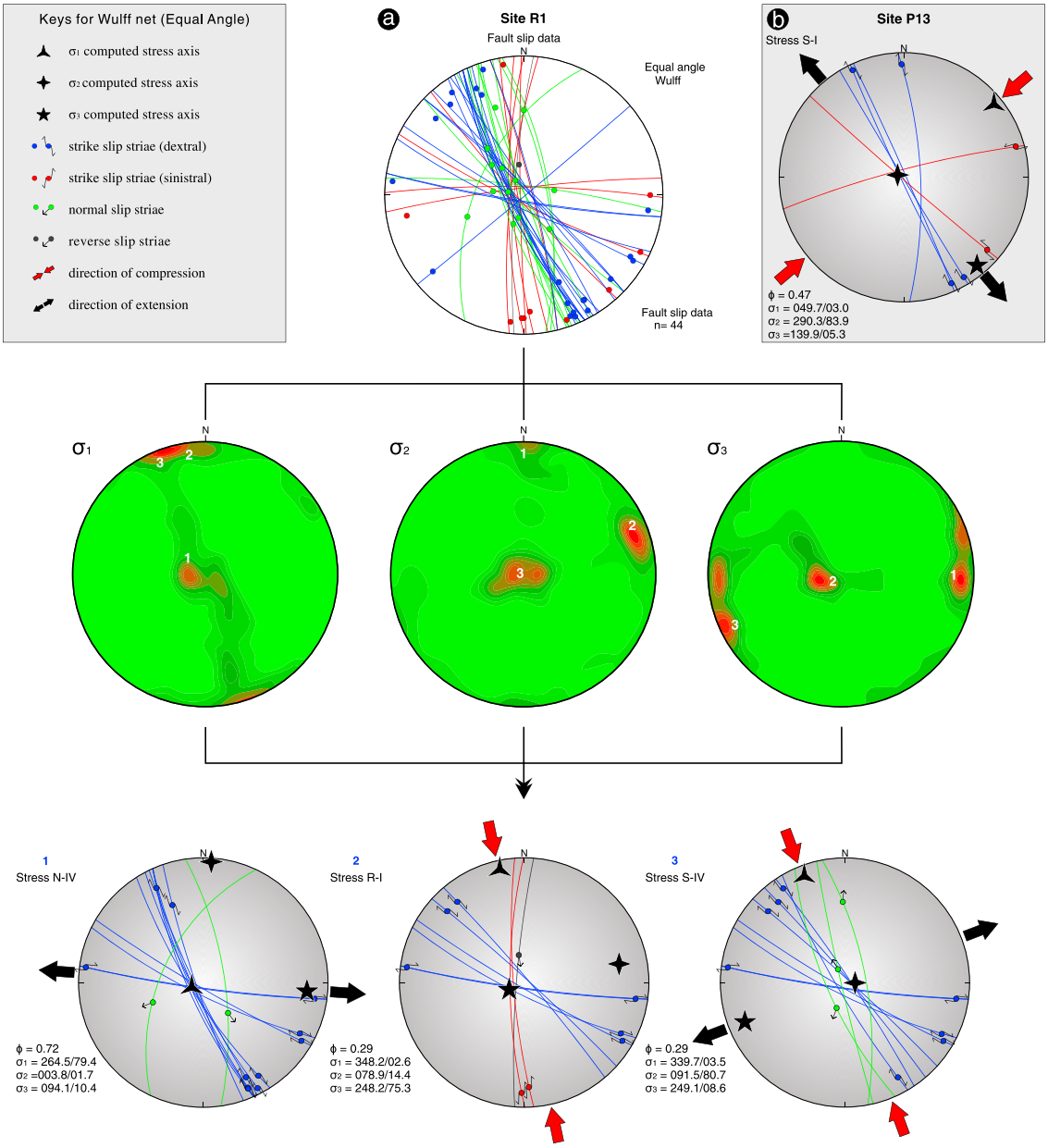

Figure 4. Example of a single phase and polyphase fault-striae data sets. (a) By applying the multiple inverse method in 9D space to the measurements collected from site R1, three deformation regimes were observed: (1) an extension regime with a ~E-W striking σ_3, (2) a reverse regime with a NNW-SSE striking σ_1, and (3) a strike-slip regime with a NNW-SSE trending σ_1. (b) Kinematic analysis of fault slip data collected from site P13 revealed only a main stage of deformation corresponding to a strike-slip regime with computed σ_1 trending NE-SW. All stereoplots are equal-angle lower hemisphere projections (Wulf net), except that the density contour stereoplots are Schmidt equal-area projections, lower hemisphere.

Getting consistent category of stress states derived from different rock ages across different scales of space in the Earth's crust is a good argument for relating them to a common regional stress field [e.g., *Saintot et al.*, 2011; *Sippel et al.*, 2009]. The consistent category of stress states has been attributed to the age of the youngest deformed rocks that has preserved the relevant fault slip data. This information, together with a relative chronology of the cross-cutting relationship, allowed to distinguish the successive tectonic events that have characterized the study area.

4. Inversion Results

Using the method mentioned above, a number of 121 local stress tensors explaining 1971 fault/striae pairs were determined for 51 localities. Results of paleostress analysis of the faults around the study areas are

shown in the supporting information (Table S1). An overview of the resulting stress regimes, most of the stress tensors together reveals that a series of clustered subvertical and subhorizontal kinematic axes agree with an Andersonian state of stress [*Anderson*, 1942]. Accordingly, 65 out of 121 tensors correspond to strike-slip regimes (subvertical σ_2), 32 to extensional stress regimes (subvertical σ_1), and 24 to compressional stress regimes (subvertical σ_3). The strike-slip stress states are therefore predominant.

After this general view, the stress tensors of each regime (strike slip, extensional, and compressional) were classified quite separately in several categories based on similarity of principal stress axis orientations. For each obtained category, the mean vector of principal stress axes is calculated via cluster analysis in Spheristat software [*Stesky and Pearce*, 1995] and all relevant φ values are represented by a single fluctuation histogram with an interval of 0.1. The standard deviation was used to summarize the distribution of values around the mean and to evaluate the validity of the results. In general, lower standard deviation values indicate a narrow spread of data around the mean, while higher values indicate more variability. The relevant fault slip data were finally compiled together into one data set and projected with a relevant mean stress vector on the lower hemisphere of the Wulff stereonet in Figure 5, 7, and 9.

4.1. Strike-Slip Stress Regimes

The largest number of paleostress states detected along the measurement sites belongs to strike-slip stress states with subvertical σ_2 axes and subhorizontal σ_1 and σ_3 axes. Nearly every site is affected by a strike-slip stress regime either as dominant or as subordinate stress state. The detected strike-slip regimes vary in the orientation of the σ_1 and σ_3 (Figure 5), exposing four distinct modes of compression (σ_1) in NE-SW, NW-SE, ~E-W, and ~N-S directions, the latter occurring less frequently.

4.1.1. NE-SW Compression (S-I)

A strike-slip stress regime with a NE-SW oriented σ_1 is the most important tectonic regime that has affected the southwestern part of Jordan. It was defined by 21 tensors (32.3% of the total calculated strike-slip stress states) and observed in 21 field stations out of a total of 51 (Table S1). The frequency distribution of respective stress ratios (φ) indicated mainly high stress ratios with an average φ value of 0.76 (Figure 5a); the regime is intermediate between pure strike slip ($\varphi = 0.5$) and transtension ($\varphi = 1$). Generally, this regime has a mean direction of compression (σ_1) trends at N50°E and a standard deviation roughly 0.05 (Table 1). A very low standard deviation indicates that the distributions of the σ_1 axes tend to be clustered together well. In contrast, the standard deviation of respective stress ratios (φ) is relatively very high (0.24), indicating a wide spread of φ values around the mean and hence some heterogeneity in the stress regime. The associated fault trends reveal two main different shear directions (Figure 5a): NNW-SSE to NNE-SSW dextral (blue lines) and NE-SW to NW-SE sinistral (red lines). A wide range of sinistral strike-slip fault directions (Figure 5a) is probably most closely related to the reactivation of favorably oriented inherited faults that developed at different deformation phases. Other faults may be younger. Overall, this predominant direction of compression is consistently indicated by stress states derived from rocks of Precambrian, Upper Cretaceous, Eocene, and Pleistocene ages. According to the youngest deformed rocks, the maximum age of these stress states dates back to late Pleistocene.

4.1.2. NW-SE Compression (S-II)

A strike-slip stress regime with a NW-SE oriented σ_1 was restricted to 16 tensors (24.6% of the total calculated strike-slip stress states) observed in 16 field stations. It is characterized by a mean N318°E compressional direction with a very small standard deviation value (Table 1). The frequency distribution of respective stress ratios (φ) reflects a wide range between $\varphi = 0.1$ and $\varphi = 0.98$ with a mean value of 0.57 and a standard deviation of 0.3. Since the standard deviation is significantly high, the mean value is not a true representative of the typical value in a data set. The compatible faults with this trend of compression are mainly NNW to NNE trending sinistral and ENE to ESW trending dextral strike-slip faults (Figure 5b). A set of NNE-SSW left-lateral faults exist in site P8 that resulted from this compression (Figure 6). According to the youngest rocks that have been affected (URC formation), the relative age of this regime dates back to late Eocene or early Oligocene time. Precambrian and Upper Cretaceous rocks also recorded this tectonic event.

4.1.3. ENE-WSW to WNW-ESE Compression (S-III)

Altogether 15 tensors (23.1% of the detected strike-slip stress states) show a ~E-W oriented σ_1. They were observed in 13 field stations of different lithologic units, ranging in age from Precambrian to Eocene. Most tensors (12 out of 15) indicate trantensional deformation (Figure 5c). Other tensors indicate a pure strike-slip

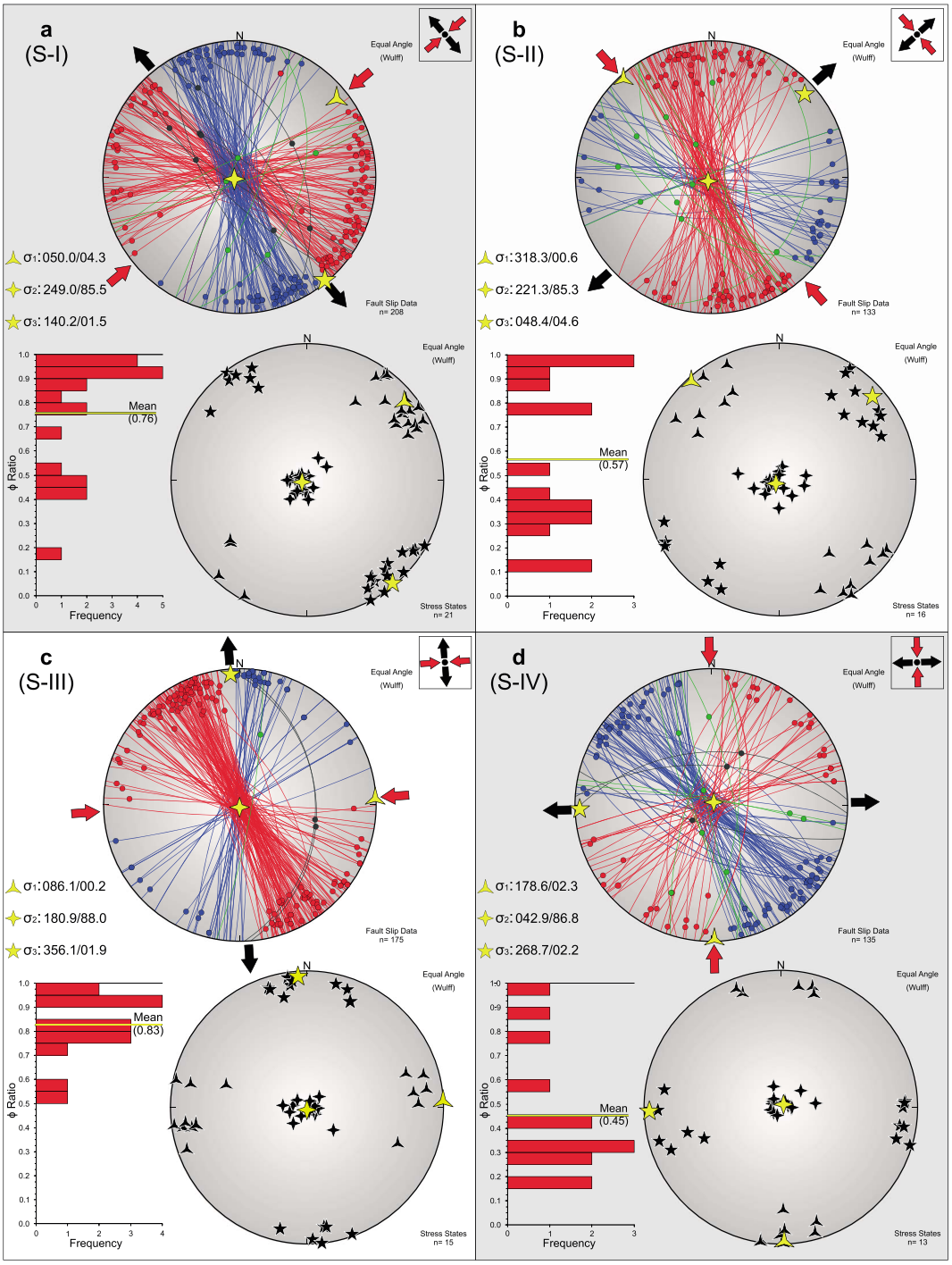

Figure 5. Strike-slip paleostress states with their stress ratios (φ) derived from fault slip data in the southwestern part of Jordan. These stress states were subdivided quite separately into four categories according to the orientation of the maximum compressional stress axes (σ_1). For each category, (1) the mean vector of principal stress axes is calculated via cluster analysis in Spheristat software [*Stesky and Pearce*, 1995], (2) all relevant φ values are represented by a single fluctuation histogram with an interval of 0.1, and (3) all associated fault slip data are compiled together into one data set and shown with a relevant mean stress vector on the lower hemisphere of the Wulff stereonet. Fault slip data are shown as plots of fault planes and striations. The majority of detected strike-slip stress states is characterized by a NE-SW oriented σ_1 (S-I). Keys for stereoplot are shown in Figure 9.

Table 1. Characteristics of Different Stress Regimes Used to Determine Tectonic Episodes as Illustrated in Figures 5, 7, and 9[a]

		σ_1	σ_1	σ_2	σ_2	σ_3	σ_3	Φ	Φ	
SS	N	M	SD	M	SD	M	SD	M^*	SD	N^*
S-I	21	050.0/04.3	0.051	249.0/85.5	0.049	140.2/01.5	0.011	0.76	0.244	208
S-II	16	318.3/00.6	0.044	221.3/85.3	0.080	048.4/04.6	0.033	0.57	0.308	133
S-III	15	086.1/00.2	0.066	180.9/88.0	0.033	356.1/01.9	0.010	0.83	0.136	175
S-IV	13	178.6/02.3	0.021	042.9/86.8	0.055	268.7/02.2	0.010	0.45	0.267	135
N-1	14	185.6/88.2	0.058	049.6/01.3	0.018	319.5/01.3	0.025	0.85	0.165	096
N-II	09	266.8/82.6	0.019	089.0/07.4	0.014	358.9/00.3	0.003	0.84	0.236	082
N-III	05	208.4/82.8	0.029	310.5/01.5	0.043	040.7/07.0	0.005	0.75	0.253	027
N-IV	04	238.1/86.2	0.011	001.2/02.1	0.004	091.4/03.2	0.009	0.79	0.113	044
R-I	14	325.7/01.8	0.013	235.7/03.0	0.044	086.9/86.5	0.045	0.34	0.280	114
R-II	07	027.0/02.9	0.009	117.4/08.4	0.012	278.2/81.1	0.014	0.58	0.262	071
R-III	03	093.9/07.7	0.006	003.0/07.0	0.003	231.3/79.6	0.010	0.65	0.399	026

[a]The stress axes for each regime are much better defined (have a much lower standard deviation) than the stress ratio φ. The following indications are reported: SS, stress states; N, number of tensors; M, mean vector computed for the main stress axes σ_1, σ_2, and σ_3 (azimuth/plunge, in degrees); SD, standard deviation; M^*, mean value computed for the stress ratio φ [$\varphi = (\sigma_2 - \sigma_3) / (\sigma_1 - \sigma_3)$]; N^*, number of explained faults by the stress state.

deformation. This means that although the same orientations for the principal stress axes are present, the relative magnitudes of the axes vary. The mean value and standard deviation for this regime of compression are given in Table 1. Faults explained by this tectonic event are mainly NNE-SSW dextral and E-W to NNW-SSE sinistral strike-slip faults (Figure 5c). The occurrence of this regime in the youngest Eocene rocks (URC unit) indicates that it prevailed at least until the ending of Eocene or the beginning of Oligocene times.

4.1.4. NNW-SSE to NNE-SSW Compression (S-IV)

A strike-slip stress regime with a ~N-S oriented σ_1 was only defined by 13 tensors (20% of the computed strike-slip stress states). It was observed in 12 field stations of different lithologic units, ranging in age from Precambrian to Pleistocene times. It is mostly associated with medium and low stress ratios (φ) with a mean

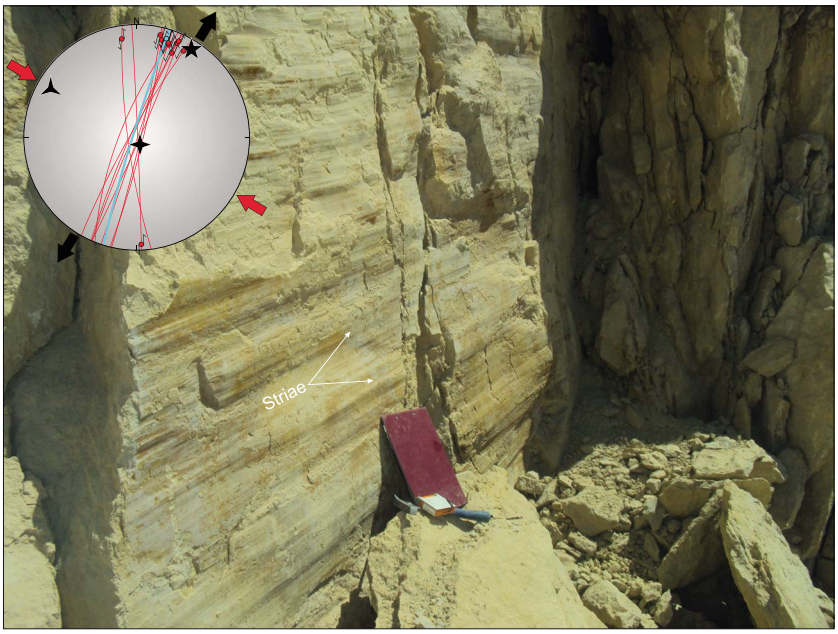

Figure 6. Large sinistral strike-slip fault with very pronounced striae cuts the Cenomanian Na'ur Limestone formation in the Wadi Musa/Petra area (site P8 in Figure 2). The fault slip datum is marked by a thick illuminated circle in the stereoplots (lower hemisphere, Wullf equal-angle stereonet). Keys of the stereoplot are the same as those in Figures 4 and 9. Paleostress inversion indicates that the strike-slip faulting resulted from an NW-SE compression (S-II) during the late Eocene-early Oligocene times.

value of 0.45 and a standard deviation of roughly 0.27. The compatible faults with this trend of compression are mainly ~NE-SW trending sinistral and ~NW-SE trending dextral strike-slip faults (Figure 5d). According to the stratigraphic ages of the affected rocks, the maximum age of this tectonic event dates back to late Pleistocene.

4.2. Extensional Stress Regimes

Extensional stress states are less common to the predominating strike-slip stress regimes (32 out of a total of 121) and are generally derived from differently aged rocks, ranging from Precambrian to Pleistocene times. They, however, show a great diversity in the orientation of the extensional stress axes (σ_3) around NW-SE, ~N-S, NE-SW, and ~E-W (Figure 7).

4.2.1. NW-SE Extension (N-I)

The extensional stress states with a NW-SE oriented σ_3 were restricted to 14 tensors (43.8% out of the 32 calculated extensional stress states). They were observed in 14 measurement sites, affecting Precambrian to Pleistocene rock units. They have a mean N319.5°E extensional direction with a very small standard deviation value. The fluctuation histogram mainly indicates high stress ratios (φ), with a mean value of 0.85 and a standard deviation of roughly 0.17, which is close to a transtensional tectonic regime. The ancient ~NW-SE and ~N-S oriented fault zones, related to the ancient tectonic deformations, were reactivated during this stress event as sinistral and dextral strike-slip faults, respectively (Figure 7a). The compatible normal faults with this tectonic event are mainly oriented in NE-SE and NNW-SSE. Since the youngest rocks documenting this trend of extension are of Pleistocene age, the computed tensional stress should be attributed to late Pleistocene.

4.2.2. ~N-S Extension (N-II)

A tensional stress regime with a mean ~N-S orientation of σ_3 axis was restricted to nine tensors (28.1% out of the calculated extensional stress states) and observed in nine measurement localities that distributed in the scattered places. It is mostly associated with high stress ratios (φ) with a mean value of 0.84 and a standard deviation of roughly 0.24 (Table 1). Similarly, this is also a normal faulting regime, with a strong transtensional character. Under this tectonic event, the ancient ~NW-SE to NNW-SSE and ~NE-SW oriented faults (Figure 7b) were reactivated as sinistral and dextral strike-slip faults, respectively. The compatible normal faults with this tectonic event are mainly oriented in ~NW-SE to NNW-SSE and ~E-W (Figure 7b). Since the youngest rocks affected by this tensional mode is of the Eocene Umm Rijam formation (URC), the maximum age of these stress states dates back to late Eocene or early Oligocene time. Upper Cretaceous rocks also show signs of an ~N-S directed extension. However, this extension is responsible for ~N-S normal faults with offsets of several matters that were observed in the Ras en Naqab area (Figure 8).

4.2.3. NE-SW Extension (N-III)

A total of five stress states show a NE-SW oriented σ_3 (15.6% of the computed normal stress states). These tensors were identified in five measurements sites, affecting Precambrian to Eocene rock units. It is mostly associated with high stress ratios (φ), over a range of values between $\varphi = 0.38$ and $\varphi = 0.99$, with a mean value of 0.75 and a standard deviation of roughly 0.25. Their faulting patterns are most probably linked to the preexisting paleofaults and represented as ~N-S oriented sinistral and ~NE-SW oriented dextral strike-slip faults as well as ~N-S to NE-SW normal faults (Figure 7c). According to the stratigraphic position of the affected rocks (Eocene Umm Rijam formation), the maximum age of these stress states dates back to late Eocene or early Oligocene time.

4.2.4. ~E-W Extension (N-IV)

In addition to the previously introduced tensional stress states, a few tensional stress states (four out of 32) show a mean ~E-W orientation of σ_3 axis. They have high stress ratios (φ) with a mean value of 0.79 and a standard deviation of roughly 0.11.

Under this stress event, the ~NE-SW and ~NW-SE oriented faults most probably reworked as sinistral and dextral strike-slip faults, respectively (Figure 7d). The compatible normal faults with this tectonic event are mainly oriented in NW-SE to ~N-S. According to the stratigraphic position of the youngest affected rocks (Pleistocene sediment unit exposed at site M4, Figure 2), the maximum age of these stress states dates back to late Pleistocene.

4.3. Compressional Stress Regimes

Stress states appear more limited (24 out of a total of 121) and were observed only in a few localities. They mainly show a great diversity in the orientation of the compressional stress axes (σ_1) around NW-SE to NNW-SSE, NE-SW, and ~E-W (Figure 9).

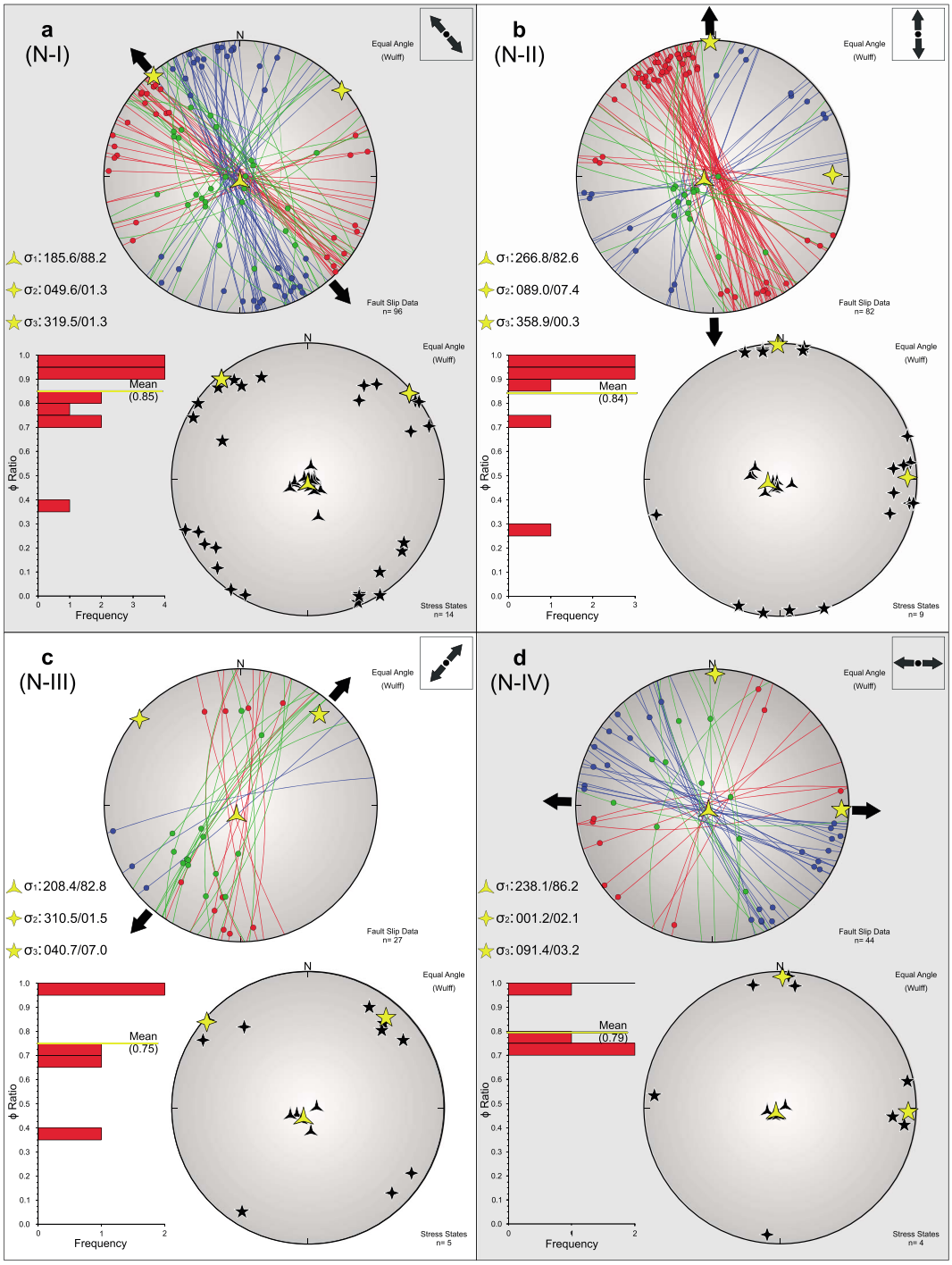

Figure 7. Extensional stress states with their stress ratios (φ) derived from fault slip data in the southwestern part of Jordan. These stress states were subdivided into four groups according to the orientation of the minimum compressional stress axes (σ_3). For each category, (1) the mean vector of principal stress axes is calculated via cluster analysis in Spheristat software [*Stesky and Pearce*, 1995], (2) all relevant φ values are represented by a single fluctuation histogram with an interval of 0.1, and (3) all associated fault slip data are compiled together into one data set and shown with a relevant mean stress vector on the lower hemisphere of the Wulff stereonet. Keys for stereoplot are shown in Figure 9. The conspicuous occurrence of strike-slip faults can be explained by the following statements. One interpretation is that the maximum principal stresses (σ_1 axes) were not quite vertical when slip occurred which can result in the development of transtension (oblique-slip) faulting. In addition, the respective stress ratios (φ) are mostly high values which indicate a transtensional tectonic environment between normal faulting and strike-slip faulting [*Delvaux et al.*, 1997]. Another interpretation is that the normal stress tensors are most likely linked to the reactivation of favorably oriented, preexisting faults. The existence of inherited fault planes of the ancient tectonic deformations can be easily reused if they are either favorably or unfavorably oriented relative to the subsequent stress regimes [*Bartholomew et al.*, 2002]. This can strongly accepted for the interested area, because of its geographical location in the near vicinity of a large-scale weakness and shear zone, i.e., late Precambrian Najd Fault System.

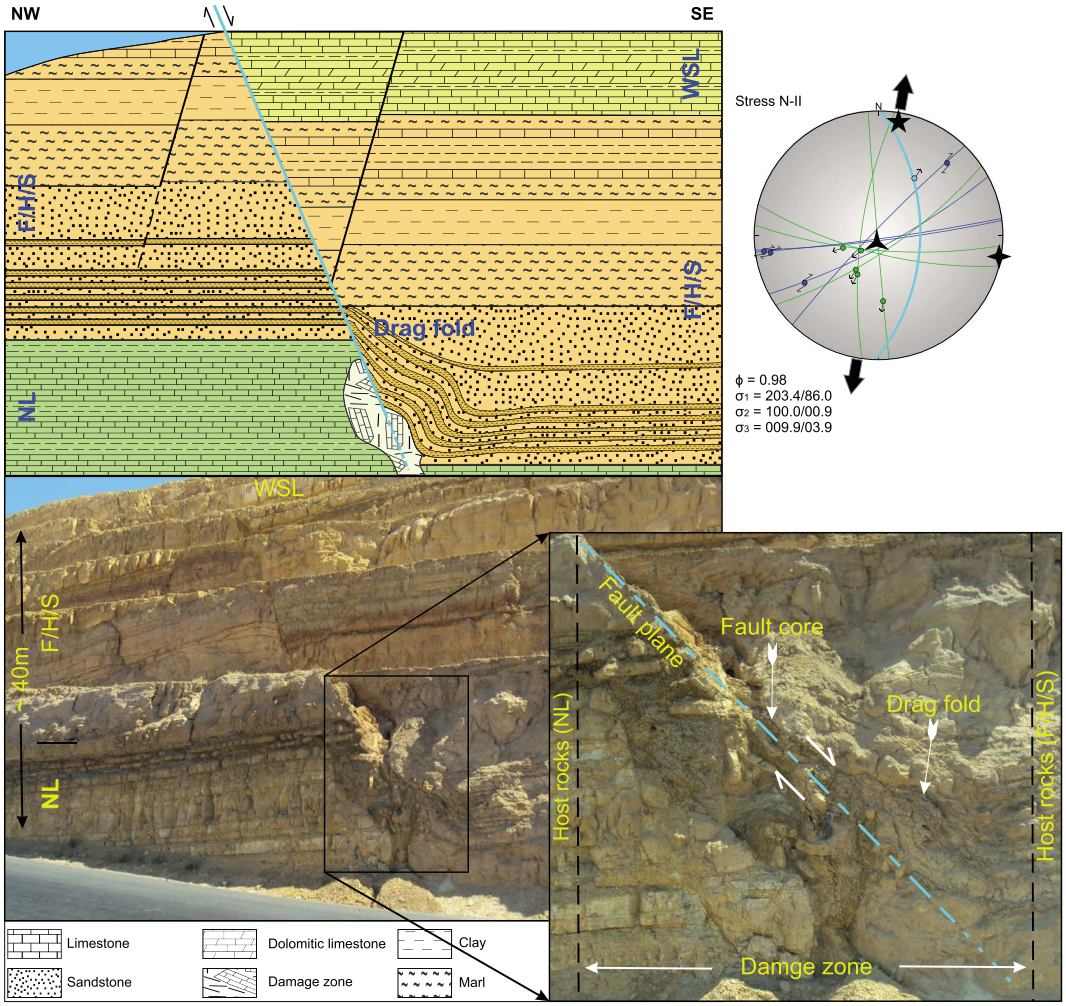

Figure 8. Geological cross section of the photograph clearly shows that the upper Cretaceous stratigraphic strata (Ajlun group) in the Ras en Naqab escarpment (sit R2, Figure 2) are mainly offset by a large normal fault. The attitude measurement of this fault is marked by a thick illuminated circle on the stereoplots (lower hemisphere, Wullf equal-angle stereonet on the upper right). Legend label is the same as it is shown in Figures 4 and 9. Paleostress inversion suggests that the normal faulting resulted from a NNE-SSW extension (N-II) during the Miocene time. The magnification image, in the lower right, shows that the occurrences of the drag fold and damage zone are caused by the normal faulting. F/H/S, undifferentiated formations of Fuheis/Hummer/Shueib (middle Cenomanian to early Turonian); NL, Na'ur Limestone formation (early Cenomanian); WSL, Wadi Es-Sir Limestone formation (Turonian).

4.3.1. NW-SE to NNW-SSE Compression (R-I)

A compressional stress regime with a NW-SE to NNW-SSE oriented σ_1 consists of 14 tensors (58.3% out of the 24 calculated compressional stress states) and was observed in 14 sites that are spread in different locations along the southwestern part of Jordan. It is characterized by a mean N325.7°E compressional direction with a very small standard deviation value. The respective stress ratios (φ) are mostly low to medium scale with a mean value of 0.34 and a standard deviation of 0.28, indicating a transpressional to pure compressional mode of deformation. The associated fracture patterns are mostly represented as NW-SE and NE-SW oriented reverse faults, NNW-SSE oriented sinistral strike-slip faults, and ~NW-SE oriented dextral strike-slip faults, taking into consideration the effect of preexisting paleofaults (Figure 9a).

The ~NW-SE reverse faults that were observed in the site P11 belong to this tectonic event (Figure 10). The youngest rock that document fault slip data related to this reverse event is of the Pleistocene unit which thus provides a maximum age for this event as a late Pleistocene. However, this direction of maximum compression is consistently indicated also by stress states derived from rocks of Precambrian, Lower Paleozoic, Upper Cretaceous, and Eocene.

4.3.2. NE-SW Compression (R-II)

The occurrence of the compressional stress regime with a NE-SW oriented σ_1 is restricted by seven tensors (29.2% out of the calculated compressional stress states) and was only recognized in seven measurement sites scattered along the area of interest. It has a mean N027°E compressional direction and a standard deviation of roughly 0.01. The respective stress ratios (φ) are covering a wide range of values with a mean value of 0.58 and a standard deviation of 0.26. Faults associated with this compression event are mainly NW-SE to ~N-S and NE-SW to ~E-W reverse faults, ~N-S oriented dextral strike-slip faults, and ~E-W oriented sinistral strike-slip faults (Figure 9b). Because the youngest rocks documenting the respective fault slip data are of the Pleistocene age, the supposed stress regime dates back to late Pleistocene time.

4.3.3. ~E-W Compression (R-III)

A compressional stress regime with a nearly E-W oriented σ_1 was only defined by three tensors (12.5% out of the computed compressional stress states) and identified at three measurement sites in the near vicinity of Petra city. The compatible fault sets are mainly NW-SE to NE-SW reverse faults, ~NW-SE oriented sinistral strike-slip faults, and NE-SW oriented dextral strike-slip faults (Figure 9c). However, this direction of contraction was not identified in rocks younger than Late Cretaceous, suggesting that a Late Cretaceous or early Eocene age for this stress event.

4.4. Tectonic Chronology

Determination of the relative timing between the different stress states represents one of the most important challenges facing the paleostress analysis. Field observations can help to provide age constraints on the timing of stress states, but they can also lead to significant mistakes [*Sperner and Zweigel*, 2010]. The stratigraphic age of the rocks that has preserved the associated fault slip data was the first two of these observations used for ordering our paleostress results. Accordingly, a compressional stress regime with a ~E-W directed σ_1 (R-III here) is the oldest tectonic event identified certainty in our analysis since the late Mesozoic. This shortening direction was obtained from fault slip data preserved within the youngest exposed rocks of the Late Cretaceous age, in the P4, P12, and P14 sites (Figure 2). The following stress events (S-II, S-III, N-II, and N-III) were calculated from fault slip data preserved within rocks of different ages including the youngest Eocene rocks. Therefore, they are considered younger than the Eocene rocks as well as the R-III event. The youngest tectonic regimes (S-I, S-IV, R-I, R-II, N-I, and N-IV) affected all exposed rocks including the Pleistocene units. Therefore, they were active during or after the Pleistocene time.

The second criterion for the relative chronology was provided, wherever possible, by the overprinting and crosscutting relationships between different striations observed on the same fault surface. The relative order between the different sets of superposed striations is often inherently ambiguous, such as in the case of two generations of differently oriented fibers lying upon each other [*Sperner and Zweigel*, 2010]. The fiber on top is often considered to be an indicator of the younger movement, but that does not necessarily have to be true because the younger fiber can develop under the older one which is dependent on the missing fault block. However, crosscutting relationships are more clear than overprinting and should be considered also if it is observed.

Despite possible pitfalls, an attempt was made to provide additional age constraints on the detected stress states based on the chronological criteria from fault surfaces. A number of fault planes, at site A3 near of Aqaba city, bear more than one generation of slickenside striae. Therefore, we could not only determine two directions of compression and one direction of extension, but also establish their relative chronology. The oldest event in this site was the ~E-W strike-slip regime (S-III), followed by the NW-SE strike-slip regime (S-II). Then, NE-SW extensional regime (N-III) happened. The superimposition of successive striae at site R3 shows that the ~E-W extensional regime (N-IV) postdated the NW-SE strike-slip regime (S-II). At site R4, two successive striations developed on several fault surfaces support that two directions of extension (N-I and N-II) have been active after the NW-SE strike-slip regime (S-II). In the Eocene URC formation at site M5, two generations of striations are related to a reactivation of the same fault plane within two different tectonic stages (Figure 11): an older generation of large corrugations (grooves) which developed under a NW-SE extensional regime (N-I) and a younger generation of striae developed under the ~N-S strike-slip regime (S-IV). At site P11, two successive striations on several fault surfaces show that the compression regime (R-I) has been active before the strike-slip regimes (S-I and S-IV). However, there is no clear evidence to arrange S-I, S-IV, N-IV, and R-II events, but generally, they have taken place at any time during the

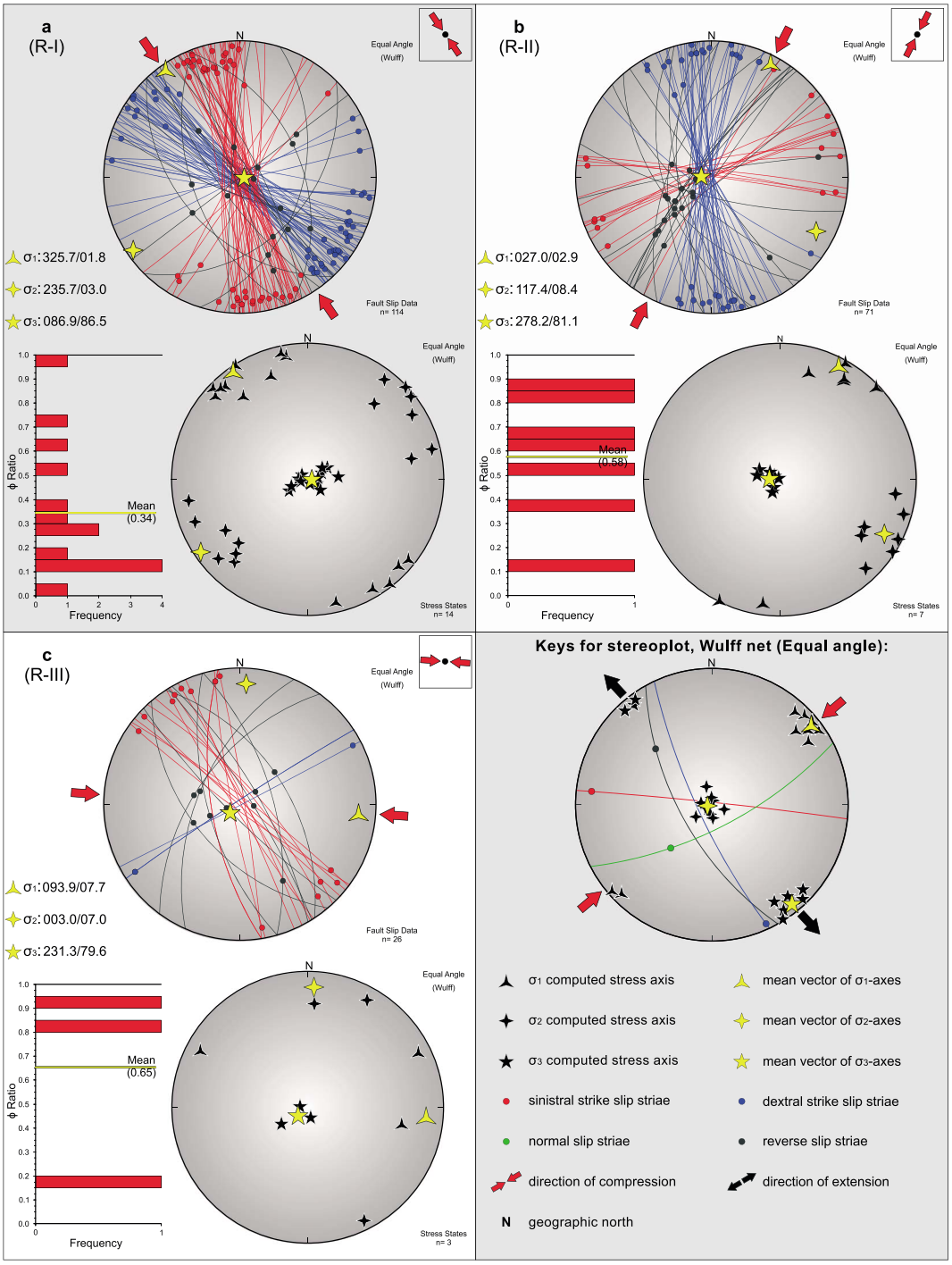

Figure 9. Compressional stress states with their stress ratios (φ) derived from fault slip data in the southwestern part of Jordan. These stress states were subdivided quite separately into three groups according to the orientation of the maximum compressional stress axes (σ_1). For each category, (1) the mean vector of principal stress axes is calculated via cluster analysis in Spheristat software [*Stesky and Pearce*, 1995], (2) all relevant φ values are represented by a single fluctuation histogram with an interval of 0.1, and (3) all associated fault slip data are compiled together into one data set and shown with a relevant mean stress vector on the lower hemisphere of the Wulff stereonet. Within the entire investigation area, the majority of detected compressional stress states is characterized by a NW-SW to NNW-SSE oriented σ_1 (R-I). Keys for stereoplot are shown in the last rectangle.

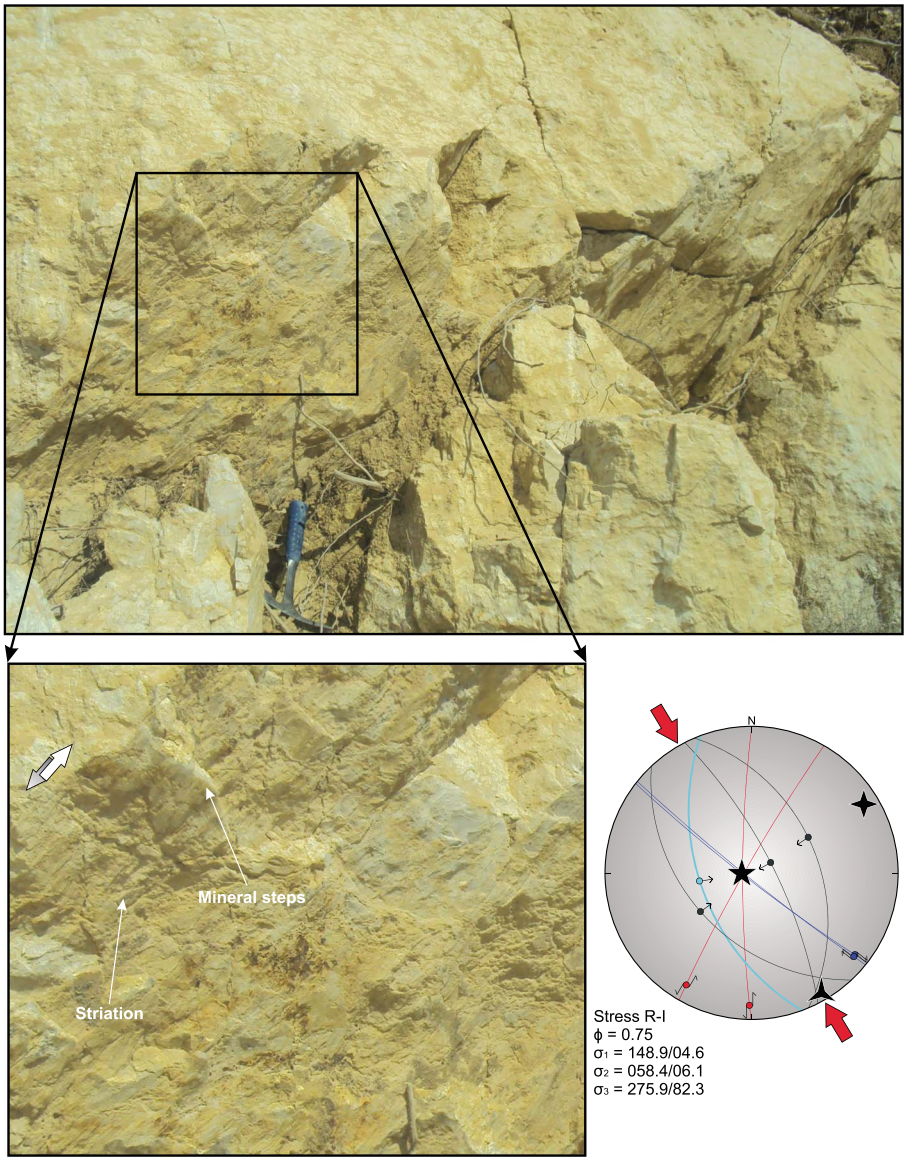

Figure 10. A reverse-slip fault with inclined striae affected the Upper Cretaceous rocks of the Wadi Musa/Petra area (site P11 in Figure 2) and corresponding stress state. The fault slip datum is indicated by a thick illuminated circle on the stereoplots (lower hemisphere, Wullf equal-angle stereonet on the lower right). Keys for stereoplot are the same as those in Figures 4 and 9.

Quaternary period. No chronological evidence was found to determine the right order to the R-I regime, but generally, it may have taken place at any time during the Quaternary period and before the strike-slip regimes (S-I and S-IV). In addition, there is no clear evidence to find the right order to N-I regime, but generally, it may have taken place at any time during the Quaternary period and before the strike-slip regime (S-IV). The relative ages between the detected stress states in the study area are summarized in Figure 12.

5. Discussion

Analysis of an extensive fault slip data collected from different sites in the southwestern part of Jordan lets us to determine various kinematic stress regimes. Based on an integration of these results with the relative chronological criteria and stratigraphical constraints, five major tectonic episodes have been determined since Late Cretaceous. Among them, four distinct compressional directions (described below) correspond

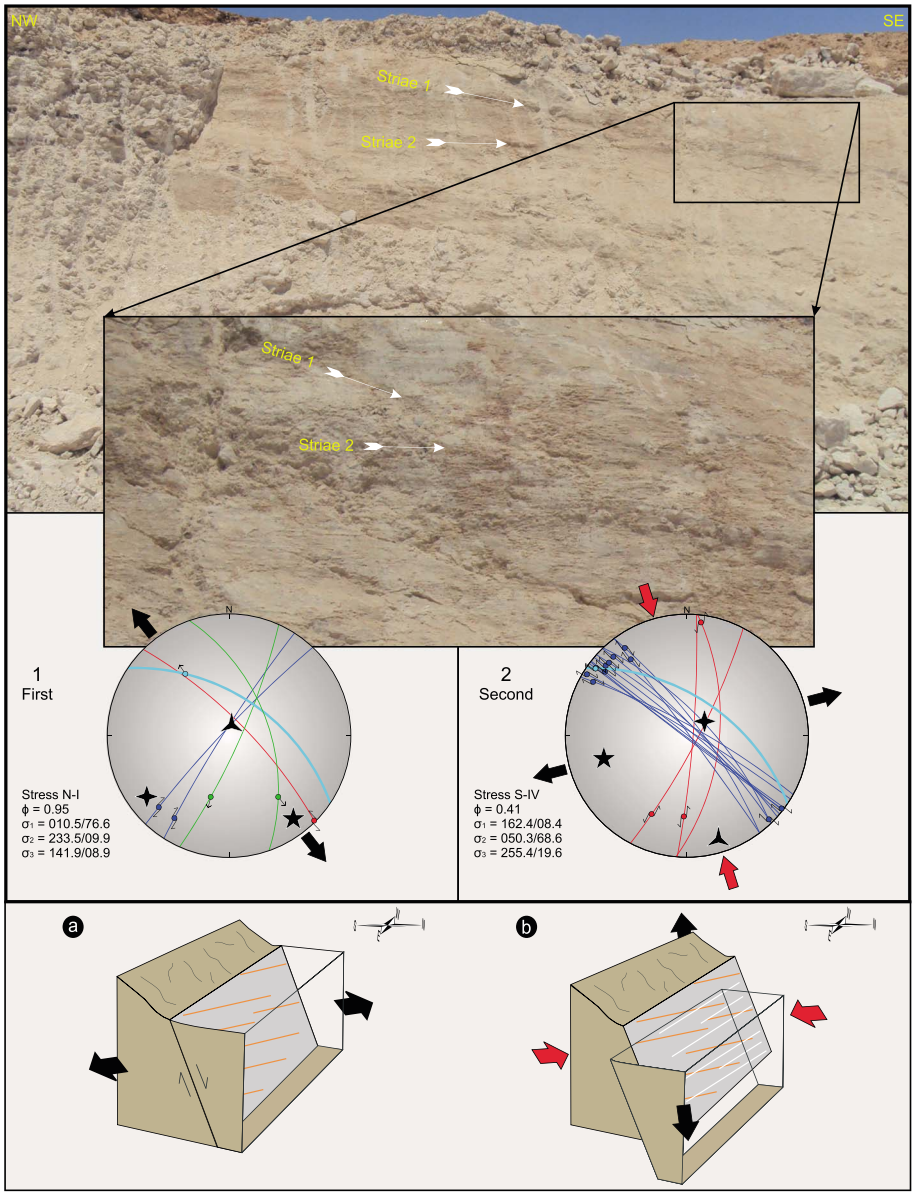

Figure 11. Crosscutting striae on a fault plane, observed in the Eocene limestone in the vicinity of Ma'an city (site M5, Figure 2). Striae sets (1) which formed by a NW-SE extension N-I are crosscut by younger striae sets (2) which generated under a NNW-SSE strike-slip regime (S-IV). The chronology here is justified [*Hippolyte et al.*, 2012], because the second movement (S-IV) was of lower magnitude than the first one which created corrugations (grooves) and was not able to erase the ridges of the corrugations. On the contrary, the striation will not detect if they were generated before the grooves. The fault datum is marked by a thick illuminated circle in the stereoplots (lower hemisphere, Wullf equal-angle stereonet). Keys for stereoplot are the same as those in Figures 4 and 9. Schemes at the bottom show a possible interpretation of the reactivation of the former normal fault by a more recent strike-slip movement. (a) NW-SE oriented extension provokes the formation of normal fault plane (gray rectangle) and leads to the first striae generation (orange lines). (b) A younger NNW-SSE strike-slip regime reactivates the preexisting fault plane and leads to the second generation of striae (white lines).

reasonably well with those observed in the northern part of the Arabian plate [*Letouzey and Tremolieres*, 1980]. The tectonic evolution of the Levant domain before and during the initial Arabia-Eurasia collision is also discussed below and summarized in Figure 13.

5.1. Composite Tectonics From Late Cretaceous to Miocene Times

The Late Cretaceous to early Cenozoic tectonic history of the Levant domain began with Syrian Arc Deformation (SAD). The SAD is associated with an ~E-W to NW-SE compressional stage in the whole

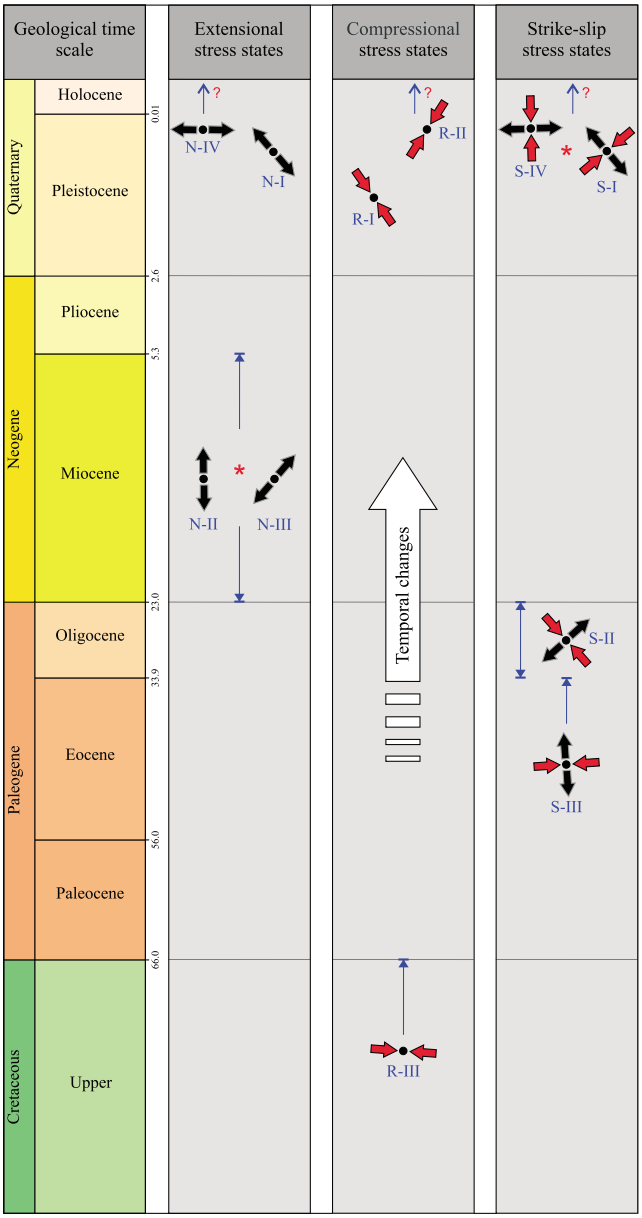

Figure 12. Chronology between local stress states in the southwestern part of Jordan. The relative age was established by the stratigraphic ages of the affected rocks and the crosscutting relationships of successive striae locally observed on the fault planes. Red asterisk indicates that no chronological evidence was found to determine the right order between the stress states. The numerical time scale from *Walker et al.* [2012]. Red and black arrows indicate the direction of compression and extension, respectively.

Levant domain [e.g., *Eyal*, 1996; *Guiraud and Bosworth*, 1999] caused by the subduction of the Neotethys beneath the Eurasian plate [e.g., *Eyal and Reches*, 1983; *Gardosh et al.*, 2008; *Garfunkel*, 1998; *Walley*, 1998]. Two main stages of Syrian Arc Deformation were identified from the characteristics of Syrian Arc folds in Lebanon and its surrounding area by *Walley* [1998]: Syrian Arc I during Coniacian to Santonian times was followed by a Syrian Arc II during late Eocene to late Oligocene times.

Our paleostress determinations reveal that the oldest brittle event recorded by us in the southwestern part of Jordan is an ~E-W tectonic compression (mode R-III here). This shortening direction was obtained only from fault slip data of the early Late Cretaceous rocks. Moreover, the paleostress analysis presented in Figure 5c shows another ~E-W compressional direction (S-III here) that affected the youngest exposed rocks of the

Eocene age. The similarity in the direction of maximum compression (σ_1) for strike-slip and compressional regimes (S-III and R-III) suggests that they can be grouped with each other as a single tectonic episode through a permutation between the σ_2 and σ_3 principal stresses. Such a permutation is a common phenomenon in brittle tectonics and has been widely described by several authors [e.g., *Angelier et al.*, 2008; *Bergerat et al.*, 2000; *Garcia et al.*, 2002; *Hu and Angelier*, 2004]. Consequently, we associate the previous regimes of compression with a single tectonic episode (first episode) characterized by approximately east-west compression which prevailed until the late Eocene (Figure 13a). This compression has been recognized in Israel [*Hardy et al.*, 2010] with a Paleocene age and was already reported, with a Late Cretaceous age, in several studies over the Levant area [*Al-Khatib et al.*, 2010; *Atallah et al.*, 2002; *Burdon*, 1959; *Diabat*, 2007; *Diabat et al.*, 2004; *Eyal*, 1996; *Mikbel and Zacher*, 1981; *Zain-Eldeen et al.*, 2002].

The next major tectonic episode (Figure 13b) is characterized by NW-SE strike-slip tectonic regime (S-II here) and prevailed at least until the ending of the first episode (late Eocene to late Oligocene times). This compressional direction corresponds to the late Eocene to pre-middle Oligocene (second phase) in the northwestern side of the Arabian plate by *Letouzey and Tremolieres* [1980] and was already reported by *Burdon* [1959] and *Salameh and Zacher* [1982] with a late Oligocene age. *Zain-Eldeen et al.* [2002] suggested a late Eocene age for this compression direction. Such a NW-SE compression direction was also recognized in the Gilboa region of the northern part of Israel by *Hatzor and Reches* [1980] and interpreted as a tectonic event accompanying to the SAD since the Miocene time. *Hardy et al.* [2010] suggested a late Miocene age for this compression direction.

Interestingly, the Late Cretaceous to Paleogene NNE and NE-trending folds in the southwestern part of Jordan [*Barjous and Mikbel*, 1990] may support the NW-SE compressional direction reported here. However, the two compression episodes mentioned here are leading to the development of the Syrian Arc features in Jordan and Israel [e.g., *AL-Hseinat*, 2009; *Barjous and Mikbel*, 1990; *Hardy et al.*, 2010] and are most probably related to the closure of the Neotethys Ocean between the Afro-Arabian and the Eurasian plates. The late Oligocene-early Miocene marks a significant change in the tectonic conditions toward the extensional tectonic sittings, resulting mainly in the initiation of the Red Sea Rift [*Guiraud and Bosworth*, 1999; *McQuarrie et al.*, 2003; *Schattner et al.*, 2006] which represents the onset of the latest episode of Gondwanaland disintegration [*Avni et al.*, 2012]. This induces a change in the velocity of Arabia plate from 3.0 to 1.1 cm/yr at ~25 Ma (Figures 13c and 13e).

The Red Sea Rift was accompanied by NE-SW extension [e.g., *Bosworth et al.*, 2005] and associated with uplift and extensive erosion [e.g., *Bender*, 1975]. The lack of the sedimentary successions and exposure of the underlying basement rocks in the Red Sea hills is related to this activity [*Amer et al.*, 2012]. The northwestern continuation of the Red Sea Rift toward the Mediterranean Sea, as a result of the NNE-SSW extension, created the Suez Rift [*Lyberis*, 1988]. Several authors proposed two main phases of an extensional history in the Red Sea Rift [e.g., *Guennoc et al.*, 1990; *Hempton*, 1987; *Lowell and Genik*, 1972; *Thisse et al.*, 1983]. The first opening stage started in the early Miocene and was accompanied by a series of continental thinning and stretching with dike injection that provoked the reactivation of the preexisting structural elements, such as the late Proterozoic Najd Shear Fault System [e.g., *Moustafa*, 1997]. The second opening stage commencing in the Pliocene to recent time is characterized by the formation of a true seafloor spreading toward the present-day configuration of the Red Sea.

In our paleostress analysis presented here, the tectonic setting of the study area changed from being compressional/strike-slip stress regimes (Syrian Arc Deformation) to an extensional regime, possibly due to the opening of the Red Sea-Suez Rift (Figure 13c). The relative chronology discussed before (see section 4.4) supports this change, because it indicates that the extensional regime postdates the Late Cretaceous to late Oligocene compressional regimes. Accordingly, two directions of extension prevailed during at least the early Miocene, NNE-SSW and NE-SW extension regimes (N-II and N-III events). Because we have no chronological evidence to order them, we believe that a rotation of the stress axes in the horizontal plane could be involved, resulting in the occurrence of both NNE-SSW and NE-SW trends of extension. In more detail, we argue that these trends of extension are part of a single major extensional regime, characterized by a high mean of stress ratios ($\varphi = 0.8$), and are likely to be related to the ongoing rifting along Red Sea-Suez since the early Miocene time (third episode). The NE-SW extension reported here was also recognized in Israel [*Hardy et al.*, 2010] and in the Gulf of Suez [*Bosworth and Steckler*, 1997] and was active during the Neogene times. *Hardy et al.* [2010] and *Homberg et al.* [2010] suggested a pre-Miocene age for the N-S extension.

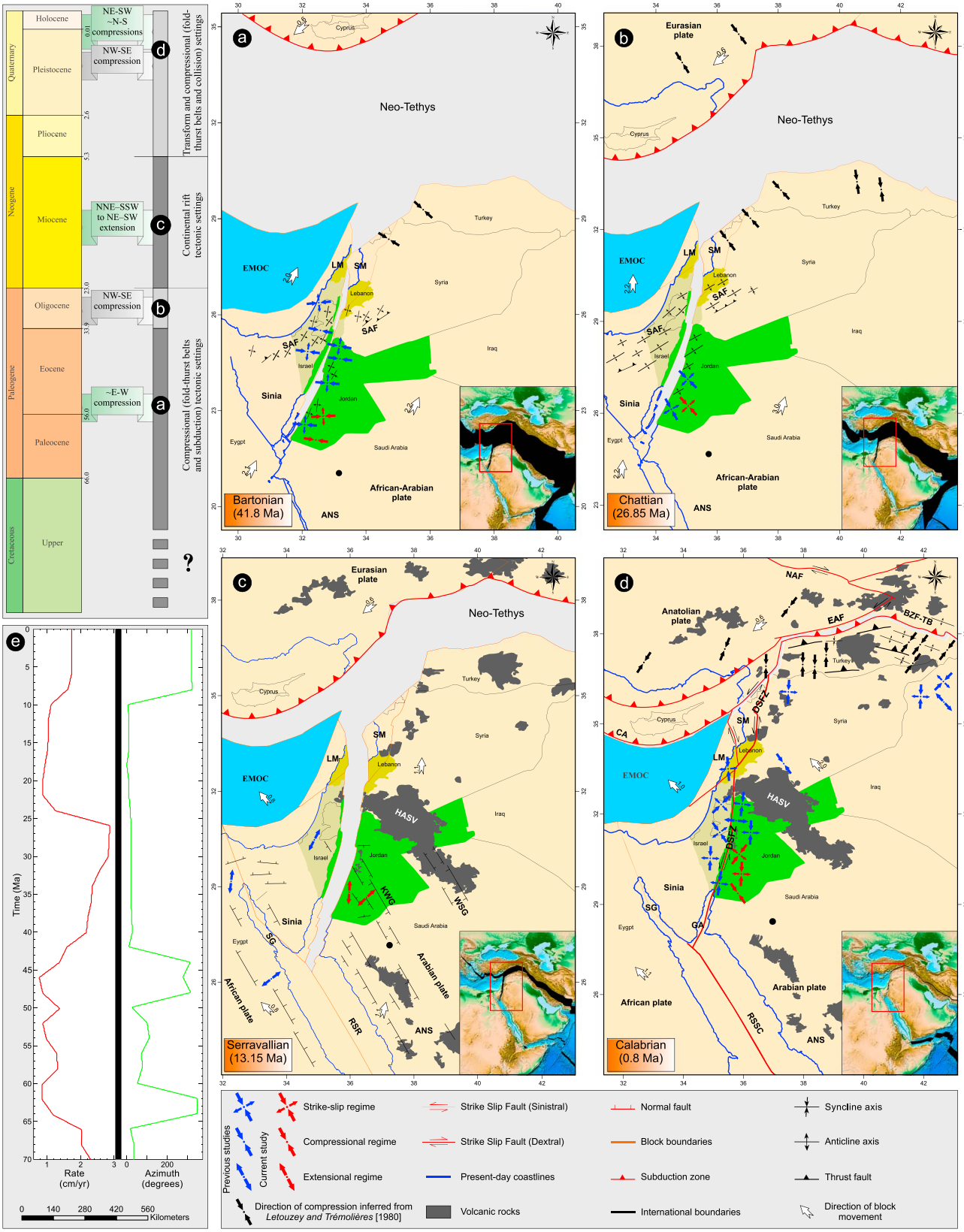
Quaternary
Holocene
Pleistocene
Neogene
Pliocene
Miocene
Paleogene
Oligocene
Eocene
Paleocene
Cretaceous
Upper
NE-SW ~N-S compressions
NW-SE compression
NNE–SSW to NE–SW extension
NW-SE compression
~E-W compression
Transform and compressional (fold-thrust belts and collision) settings
Continental rift tectonic settings
Compressional (fold-thrust belts and subduction) tectonic settings
Neo-Tethys
Eurasian plate
African-Arabian plate
Arabian plate
African plate
Anatolian plate
Sinia
EMOC
LM
SM
SAF
HASV
KWG
WSG
SG
RSR
RSSC
NAF
EAF
BZF-TB
DSFZ
CA
ANS
Bartonian (41.8 Ma)
Chattian (26.85 Ma)
Serravallian (13.15 Ma)
Calabrian (0.8 Ma)
Time (Ma)
Rate (cm/yr)
Azimuth (degrees)
Kilometers
Strike-slip regime
Compressional regime
Extensional regime
Direction of compression inferred from Letouzey and Trémolières [1980]
Strike Slip Fault (Sinistral)
Strike Slip Fault (Dextral)
Present-day coastlines
Volcanic rocks
Normal fault
Block boundaries
Subduction zone
International boundaries
Syncline axis
Anticline axis
Thrust fault
Direction of block movement
Previous studies
Current study

Figure 13

5.2. Pliocene to Recent Tectonics

The late Cenozoic tectonic activity of the Levant area was mainly associated with the initiation of the dextral movement along the North Anatolian Fault (NAF), the sinistral movement along both the Dead Sea Fault Zone (DSFZ) and the East Anatolian Fault (EAF), and creation the Gulf of Aqaba [e.g., *Garfunkel*, 1981, 2014; *Garfunkel and Ben-Avraham*, 1996; *Hempton*, 1987]. Abrupt change in the direction of Arabia plate motion from ~N to NW at 8 Ma was reported with a constant plate velocity of ~2 cm/yr between 8 and 0 Ma (Figures 13d and 13e).

Our chronology analyses clearly indicate that the tectonic setting of the study area changed from being an extensional regime toward a period that was mainly dominated by compressional/strike-slip stress regimes. Accordingly, three directions of compression were observed in late Cenozoic times trending NW-SE, ~N-S, and NE-SW oriented σ_1 (R-I, S-IV, R-II, and S-I regimes here), the latter is the most common in the study area (Figure 13d). The chronological relationships reveal that the NW-SE compressional event (R-I) predates both the ~N-S and NE-SW strike-slip regimes (S-IV and S-I, respectively). Unfortunately, no clear chronological evidence was found in the field to distinguish between ~N-S and NE-SW strike-slip regimes, but generally, they have taken place at any time after the NW-SE compression (R-I). Besides these trends of compression, an important extensional regime with a NW-SE oriented σ_3 (N-I here) and a minor striking of E-W extension (N-IV here) were also observed in late Cenozoic times.

The NW-SE compression recognized in this study (R-I here) was derived from fault slip data of the youngest Pleistocene age, suggesting a late Pleistocene for this stress event (forth episode). This shortening direction is very well known within the Palmyride fold zone in the central Syria [*Darkal*, 2003] and corresponds to the late Neogene compressional event that accompanied the shortening and uplifting of the Palmyrides. It is somewhat similar to the late Miocene NW-SE compression (third phase) in the northwestern side of the Arabian plate [*Letouzey and Tremolieres*, 1980]. It was also recognized in the northwest Syria [*Al-Abdalla et al.*, 2010] and in Lebanon [*Homberg et al.*, 2010] with Miocene age. However, this direction of compression is difficult to correlate with the major structures found in Jordan, but it appears to be related to the general collision between the Arabian and Eurasian plates.

The NE-SW strike-slip regime (S-I) is the most important tectonic event that has affected the southwestern part of Jordan. Because the S-I and R-II stress regimes are generally consistent in the NE-SW oriented σ_1, we interpret them as a single tectonic regime characterized by a strong NE-SW oriented compression, resulting from the easy permutations between the σ_2 and σ_3 principal stresses. The ubiquitous occurrence of NE-SW compression throughout the entire investigation area leads us to the assumption that this tectonic event belongs to a more recent deformation and most probably still active nowadays. Generally, this direction of compression seems most consistent with the oblique collision between Arabian plate and the Iranian block (Eurasian plate) and almost perpendicular to the Zagros fold-thrust belt. There are no relevant major structures found in Jordan that appear to be in an agreement with this compression. However, this compressional direction corresponds to the Plio-Quaternary NE-SW compression (fourth phase) in the northeastern side of the Arabian plate [*Letouzey and Tremolieres*, 1980]. It is recognized in Israel, as a minor compression trend, with a Neogene age [*Hardy et al.*, 2010]. It is also recognized in the northern region of Iraq by *Aljumaily and Othman* [2012] and interpreted as a major tectonic event that occurred in the late

Figure 13. Possible scenarios of tectonic evolution and paleostress patterns in the Levant domain since the Late Cretaceous: (a and b) Late Cretaceous to late Paleogene closure of Neotethyan basins between the Eurasian and Afro-Arabian plates, during which Syrian Arc fold-thrust belts developed; (c) Miocene extension resulting in the development of Red Sea rift and abundant graben systems; (d) late Cenozoic continental collision between the Arabian and Eurasian plates, during which Bitlis-Zagros fold-thrust belts and Dead Sea Fault Zone developed that represent the main present-day structure; and (e) the speed and direction of movement for the black point on the Arabian plate between 70 Ma and 0 Ma with respect to the Iranian block. The white arrows and numbers show the direction and speed of the plates. PaleoWeb v.1.1 [*Rothwell Group*, 2011] and open-source software GPlates v.1.5 (www.gplates.org) were used to reconstruct the plate tectonic of each stage since the Late Cretaceous. Red arrows indicate paleostress directions observed in this study, while black and blue arrows indicate those directions observed from the following studies [*Al-Abdalla et al.*, 2010; *Aljumaily and Othman*, 2012; *Al-Khatib et al.*, 2010; *Bosworth and Steckler*, 1997; *Darkal*, 2003; *Diabat et al.*, 2004; *Eyal*, 1996; *Hardy et al.*, 2010; *Homberg et al.*, 2010; *Letouzey and Tremolieres*, 1980; *Zain-Eldeen et al.*, 2002; *Zanchi et al.*, 2002]. Abbreviations: EMOC, Eastern Mediterranean Oceanic Crust; GA: Gulf of Aqaba; HASV, Harrat Ash Shaam Volcanic province; LM, Levantine Margin; SG, Sueze Gulf; SM, Syrian Margin; other abbreviations as in Figure 1.

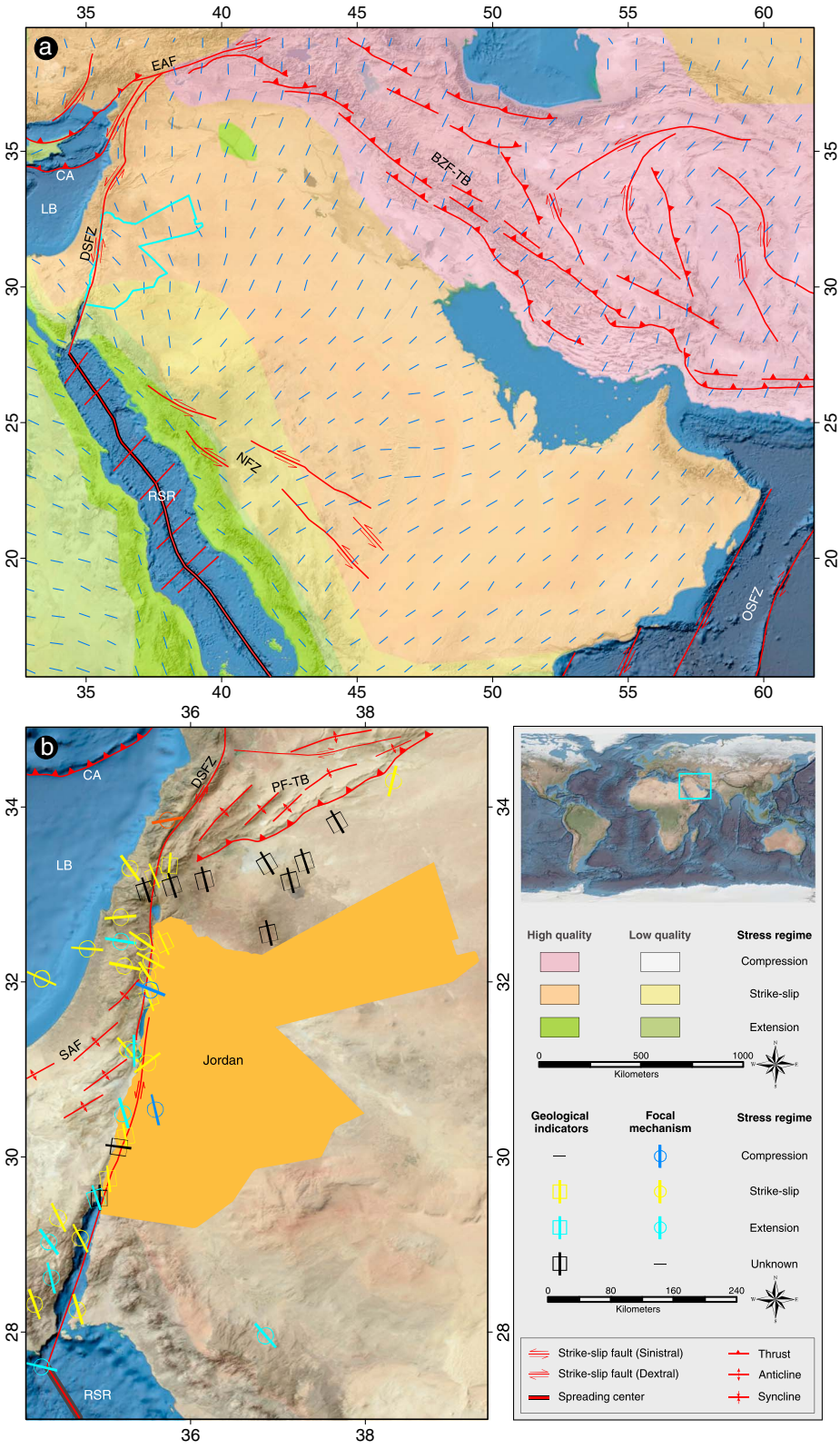

Figure 14. (a) Present-day directions of maximum horizontal compressional stress of the Arabian plate and the interpreted stress environments. Map modified after J. Mattner (2009) available from the Petroleum Geoscience Consultant (GeoTech), Kingdom of Bahrain (http://www.geotech-bahrain.net). (b) Maximum horizontal compressional stress directions of the Dead Sea domain provided as a GIS layer by O. Hurd (2010) available from the CEUS-SSC Project (http://www.ceus-ssc.com). Both maps superimposed on the global hillshading and Blue Marble images [*Becker et al.*, 2009; *Stockli et al.*, 2005]. Abbreviations are the same as in Figure 1.

Tertiary. Additionally, we argue that the NW-SE extensional regime (N-I) closely corresponds to the NE-SW strike-slip regime (S-I). A permutation between σ_2 and σ_1 stress axis leads to a change from a strike-slip to extensional stress regime with a NW-SE trending σ_3.

An ~N-S strike-slip regime (S-IV here) is compatible with the left-lateral movement along the Dead Sea Fault Zone (DSFZ) and similar to the Plio-Quaternary N-S compression (fourth phase) in the northwestern side of the Arabian plate [*Letouzey and Tremolieres*, 1980]. A similar compression had also been noticed over the Levant area, in Jordan [*Al-Khatib et al.*, 2010; *Atallah et al.*, 2002; *Burdon*, 1959; *Diabat*, 2007; *Diabat et al.*, 2004; *Zain-Eldeen et al.*, 2002], Israel [*Eyal*, 1996; *Hardy et al.*, 2010; *Joseph-Hai et al.*, 2010], Syria [*Darkal*, 2003; *Zanchi et al.*, 2002], Lebanon [*Homberg et al.*, 2010], and Iraq [*Aljumaily and Othman*, 2012]. On the other hand, the minor E-W extension (N-IV) is closely related to the ~N-S strike-slip regime (S-IV), due to σ_1 and σ_2 stress permutations. The southern part of the DSFZ is marked by an almost continuous valley, 10–20 km wide, with a series of deep pull-apart basins. These structures are generally delimited by faults indicating normal displacement [*Garfunkel*, 1981]. The formation of such structures along the already active transform fault has been a subject of vigorous debate within the past years. New three-dimensional analogue modeling experiments [*Smit et al.*, 2010] suggest that the rift-like morphology of the DSFZ is a logical consequence of the change in plate kinematics ca. 5 Ma ago. A model indicates a two-stage Cenozoic tectonic evolution, comprising the following: (1) an initial phase of a sinistral strike-slip shear zone affected the whole lithosphere with a total displacement of 65 km, which lasted from 13 to 5 Ma; and (2) a subsequent rifting phase, starting at 5 Ma, has led to the conspicuous changes in the surface morphology and structure in the southern segment of the DSFZ. The identification of two distinct compressional trends in the current study, namely, ~N-S (S-IV) and NW-SE (R-I), with a minor striking of E-W extension (N-IV) in late Cenozoic times strongly supports this model.

The distribution of the present-day maximum horizontal compression (Figure 14a) shows an ~N-S and NE-SW oriented alignments in the north of the Arabian plate. These trends correspond respectively to the trend of the ~N-S and NE-SW oriented compressions (fifth episode) that were observed in this study. Moreover, NW-SE orientations (blue and cyan lines) of the maximum horizontal compressive stress in the Dead Sea domain (Figure 14b) correspond respectively to the Quaternary NW-SE oriented compression (R-I) and NW-SE oriented extension (N-I) that were reported in this study.

However, the identification of five paleostress episodes in this study supports previous suggestion that the evolution of area is coupled to a system of multi-paleostress events [*Bahat et al.*, 2007] rather than by two major paleostress events [*Eyal and Reches*, 1983; *Eyal*, 1996].

6. Conclusions

The present study shows a polyphase tectonic deformation for the southwestern part of Jordan since Late Cretaceous times until the present day. The reactivation of preexisting structures played a significant role on fracture development in younger strata of this region. Most paleofaults that originated in the pre–late Mesozoic are perhaps reactivated during the Cenozoic. A new approach for the paleostress tensor reconstruction with a new fault slip data enables us to identify five major tectonic episodes, which were mostly recognized by *Letouzey and Tremolieres* [1980] and *Zain-Eldeen et al.* [2002]. The oldest tectonic event has been certainly identified in our analysis since the late Mesozoic to late Eocene belong to the compressional/strike-slip stress regime with ~E-W trending σ_1. The next major tectonic event belongs to the strike-slip stress regime with NW-SE oriented σ_1 and prevailed at least until the ending of the first episode (late Eocene to late Oligocene). Both compressional events are responsible for the development of the Syrian Arc fold-thrust belts in Jordan and its surrounding areas. The early Miocene marks a conspicuous change in the paleostress history of the study area toward an extensional tectonic setting with NNE-SSW to NE-SW trending σ_3, most possibly in response to the ongoing rifting along Red Sea-Suez axis and the breakup of the Afro-Arabian plate. Late Cenozoic shows the occurrence of another transitional stage in the tectonic conditions of the region. It is mainly characterized by a period of tectonic instability, marked mainly by an older NW-SE and younger ~N-S and NE-SW compressions. Besides these trends of compression, an important extensional event with NW-SE oriented σ_3 and a minor striking of E-W extension were also observed. The NW-SE compressional regime is very well known within the Palmyride fold zone in the central Syria and corresponds to the late Neogene compressional event that accompanied the shortening and uplifting of

the Palmyrides. The prevailing compressional/strike-slip regime with a NE-SW oriented σ_1, which is often accompanied with a NW-SE extension, is consistent with the oblique collision between Arabian plate and Iranian block (Eurasian plate) and almost perpendicular to the Zagros fold-thrust belt. The ~N-S strike-slip regime, which is often accompanied with an E-W extension, is consistent with the northern collision between Arabian and Eurasian plates and almost perpendicular to the Bitlis suture zone. The late Cenozoic paleostress patterns, however, are in good agreement with the present-day stress.

Acknowledgments
Data supporting Figures 1 and 14 are available at (1) NASA's Visible Earth. Data set: Blue Marble. Data set name: world.topo.bathy.200410.3x21600x21600.C1.jpg. (2) e-Atlas Australia's Tropical Land and Seas. Data set: SRTM30-plus_v8. Data set name: World_e-Atlas-UCSD_SRTM30-plus_v8_Hillshading.tif.

References

Al-Abdalla, A., E. Barrier, A. Matar, and C. Müller (2010), Lattakia Basin and tectonic evolution of the Arabian platform in NW Syria, in *Evolution of the Levant Margin and Western Arabia Platform since the Mesozoic*, edited by C. Homberg et al., *Geol. Soc. London Spec. Publ.*, *341*, 1–8.

Alavi, M. (1991), *Tectonic Map of the Middle East, Scale 1:5,000,000*, Geol. Surv. of Iran, Iran, Tehran.

AL-Hseinat, M. (2009), Structural analysis of the Wadi Shueib Fold Belt, Jordan, MSc thesis, Dep. of Earth and Envi. Sci., Yarmouk Univ., Irbid, Jordan.

Aljumaily, I. S., and N. M. A. Othman (2012), Structural analysis of brittle failure structures in Spi Res Anticline – Northern Iraq, *Iraqi Nat. J. Earth Sci.*, *12*(2), 43–78.

Al-Khatib, N., M. Atallah, and A. Diabat (2010), Paleostress analysis of the Cretaceous rocks in northern Jordan, *Jordanian J. Earth Environ. Sci.*, *3*(1), 25–36.

Amer, R., M. Sultan, R. Ripperdan, and J. Encrancian (2012), Structural architecture for development of marginal extensional subbasins in the Red Sea active rift zone, *Int. J. Geosci.*, *3*(1), 133–152, doi:10.4236/ijg.2012.31016.

Anderson, E. M. (1942), *The Dynamics of Faulting and Dyke Formation with Applications to Britain*, Oliver and Boyd, Edinburgh.

Angelier, J. (1979), Determination of the mean principal directions of stress for a given fault population, *Tectonophysics*, *56*(3–4), T17–T26, doi:10.1016/0040-1951(79)90081-7.

Angelier, J. (1989), From orientation to magnitudes in paleostress determinations using fault slip data, *J. Struct. Geol.*, *11*(1–2), 37–50, doi:10.1016/0191-8141(89)90034-5.

Angelier, J. (1990), Inversion of field data in fault tectonics to obtain the regional stress—III. A new rapid direct inversion method by analytical means, *Geophys. J. Int.*, *103*(2), 363–376, doi:10.1111/j.1365-246X.1990.tb01777.x.

Angelier, J., F. Bergerat, R. Stefansson, and M. Bellou (2008), Seismotectonics of a newly formed transform zone near a hotspot: Earthquake mechanisms and regional stress in the South Iceland Seismic Zone, *Tectonophysics*, *447*(1–4), 95–116, doi:10.1016/j.tecto.2006.07.016.

Atallah, M., T. M. Niemi, and H. Mustafa (2002), *Deformation at a Strike-Slip, Stepover Zone Along the Southeastern Margin of the Dead Sea Pull Apart Basin, Jordan*, *EGU Stephan Mueller Spec. Publ. Ser.*, vol. 2, pp. 49–62, Copernicus Publ. on behalf of the European Geosciences Union (EGU), Göttingen, Germany.

Avni, Y., A. Segev, and H. Ginat (2012), Oligocene regional denudation of the northern Afar dome: Pre- and syn-breakup stages of the Afro-Arabian plate, *Geol. Soc. Am. Bull.*, *124*(11–12), 1871–1897, doi:10.1130/B30634.1.

Baer, G., and Z. Reches (1989), Doming mechanisms and structural development of two domes in Ramon, southern Israel, *Tectonophysics*, *166*(4), 293–315, doi:10.1016/0040-1951(89)90282-5.

Bahat, D., V. Frid, and A. Rabinovich (2007), Paleostress clockwise rotation in the Sinai–Israel sub-plate and the initiation of the Dead Sea Rift, *Isr. J. Earth Sci.*, *55*, 159–171.

Barjous, M., and S. Mikbel (1990), Tectonic evolution of the Gulf of Aqaba-Dead Sea transform fault, *Tectonophysics*, *180*(1), 49–59, doi:10.1016/0040-1951(90)90371-E.

Bartholomew, M. J., M. C. Stickney, E. M. Wilde, and R. G. Dundas (2002), Late Quaternary paleoseismites: Syndepositional features and section restoration used to indicate paleoseismicity and stress-field orientations during faulting along the main Lima Reservoir fault, southwestern Montana, in *Ancient Seismites*, edited by F. R. Ettensohn et al., *Geol. Soc. Am. Spec. Pap.*, *359*, 29–47.

Becker, J. J., et al. (2009), Global bathymetry and elevation data at 30 arc seconds resolution: SRTM30_PLUS, *Mar. Geod.*, *32*(4), 355–371, doi:10.1080/01490410903297766.

Beicip (1981), *Structural Map of Jordan*, scale 1:5,000,000, Geological Mapping Division, Natural Resources Authority, Amman, Jordan.

Ben-Avraham, Z. (1989), Multiple opening and closing of the eastern Mediterranean and south China basins, *Tectonics*, *8*(2), 351–362, doi:10.1029/TC008i002p00351.

Bender, F. (1975), Geology of the Arabian Peninsula: Jordan, *U.S. Geol. Surv. Prof. Pap.*, *560–1*, Washington, D. C.

Bergerat, F., J. Angelier, and C. Homberg (2000), Tectonic analysis of the Husavik-Flatey Fault (northern Iceland) and mechanisms of an oceanic transform zone, the Tjörnes Fracture Zone, *Tectonics*, *19*(6), 1161–1177, doi:10.1029/2000TC900022.

Bosworth, W., and M. R. Steckler (1997), Stress field changes in the Afro-Arabian rift system during the Miocene to recent period, *Tectonophysics*, *278*(1–4), 47–62, doi:10.1016/S0040-1951(97)00094-2.

Bosworth, W., P. Huchon, and K. McClay (2005), The Red Sea and Gulf of Aden Basin, *J. Afr. Earth Sci.*, *43*(1–3), 334–378, doi:10.1016/j.jafrearsci.2005.07.020.

Bott, M. H. P. (1959), The mechanics of oblique slip faulting, *Geol. Mag.*, *96*(2), 109–117, doi:10.1017/S0016756800059987.

Brew, G. E. (2001), Tectonic evolution of Syria interpreted from integrated geophysical and geological analysis, PhD thesis, Dep. of Earth and Atmos. Sci., Cornell Univ., New York.

Burdon, D. J. (1959), *Handbook of the Geology of Jordan*, Government of the Hashemite Kingdom of Jordan, Amman.

Darkal, A. N. (2003), Tectonic evolution of the western edge of the Palmyride chain (Annabk anticline, Syria) from Paleostress data: Geodynamical implications, *Damascus Univ. J. Basic Sci.*, *19*, 59–100.

Delvaux, D. (2012), Release of program Win-Tensor 4.0 for tectonic stress inversion: Statistical expression of stress parameters, EGU General Assembly, Vienna, Geophys. Res. Abs., 14, EGU2012-5899.

Delvaux, D., and B. Sperner (2003), New aspects of tectonic stress inversion with reference to the TENSOR program, in *New Insights into Structural Interpretation and Modelling*, edited by D. A. Nieuwland, *Geol. Soc. London Spec. Publ.*, *212*, 75–100.

Delvaux, D., R. Moeys, G. Stapel, C. Petit, K. Levi, A. Miroshnichenko, V. Ruzhick, and V. San'kov (1997), Paleostress reconstructions and geodynamics of the Baikal region, Central Asia, Part 2. Cenozoic rifting, *Tectonophysics*, *282*(1–4), 1–38, doi:10.1016/S0040-1951(97)00210-2.

Diabat, A. (2007), Paleostress analysis of the Cretaceous-Tertiary rocks in central Jordan, *Dirasat Univ. Jordan*, *34*(2), 192–200.

Diabat, A. (2009), Structural and stress analysis based on fault-slip data in the Amman area, Jordan, *J. Afr. Earth Sci.*, *54*(5), 155–162, doi:10.1016/j.jafrearsci.2009.03.011.

Diabat, A., M. Atallah, and M. Salih (2004), Paleostress analysis of the Cretaceous rocks in the eastern margin of the Dead Sea transform, Jordan, *J. Afr. Earth Sci.*, *38*(5), 449–460, doi:10.1016/j.jafrearsci.2004.04.002.

Dilek, Y. (2006), Collision tectonics of the Mediterranean region: Causes and consequences, in *Postcollisional Tectonics and Magmatism in the Mediterranean Region and Asia*, edited by Y. Dilek and S. Pavlides, *Geol. Soc. Am. Spec. Pap.*, *409*, 1–13, doi:10.1130/2006.2409(01).

Dilek, Y. (2010), Eastern Mediterranean geodynamics, *Int. Geol. Rev.*, *52*(2–3), 111–116, doi:10.1080/00206810902951031.

Dilek, Y., and J. C. Rowland (1993), Evolution of a conjugate passive margin pair in Mesozoic southern Turkey, *Tectonics*, *12*(4), 954–970, doi:10.1029/93TC01060.

Doblas, M. (1998), Slickenside kinematic indicators, *Tectonophysics*, *295*(1–2), 187–197, doi:10.1016/S0040-1951(98)00120-6.

Duyverman, H. J., N. B. W. Harris, and C. J. Hawkesworth (1982), Crustal accretion in the Pan-Africa: Nd and Sr isotope evidence from the Arabian Shield, *Earth Planet. Sci. Lett.*, *59*(2), 315–326, doi:10.1016/0012-821X(82)90134-0.

Etchecopar, A., G. Vasseur, and M. Daignieres (1981), An inverse problem in microtectonics for the determination of stress tensor from fault striation analysis, *J. Struct. Geol.*, *3*(1), 51–65, doi:10.1016/0191-8141(81)90056-0.

Eyal, Y. (1996), Stress field fluctuations along the Dead Sea rift since the Middle Miocene, *Tectonics*, *15*(1), 157–170, doi:10.1029/95TC02619.

Eyal, Y., and Z. Reches (1983), Tectonic analysis of the Dead Sea rift region since the Late Cretaceous based on mesostructures, *Tectonics*, *2*(2), 167–185, doi:10.1029/TC002i002p00167.

Fisher, N. I., T. Lewis, and B. J. J. Embleton (1987), *Statistical Analysis of Spherical Data*, Cambridge Univ. Press, Melbourne, Australia.

Fox, J. E., and T. S. Ahlbrandt (2002), Petroleum geology and total petroleum systems of the Widyan Basin and interior platform of Saudi Arabia and Iraq, *U. S. Geol. Surv. Bull. 2202–E*, U.S. Dept. of the Interior, Denver, Colo.

Galli, P. (1999), Active tectonics along the Wadi Araba–Jordan Valley transform fault, *J. Geophys. Res.*, *104*(B2), 2777–2796, doi:10.1029/1998JB900013.

Garcia, S., J. Angelier, F. Bergerat, and C. Homberg (2002), Tectonic analysis of an oceanic transform fault zone based on fault-slip data and earthquake focal mechanisms: The Húsavík-Flatey Fault zone, Iceland, *Tectonophysics*, *344*(3–4), 157–174, doi:10.1016/S0040-1951(01)00282-7.

Gardosh, M., Y. Druckman, B. Buchbinder, and M. Rybakov (2008), The Levant Basin offshore Israel: Stratigraphy, structure, tectonic evolution and implications for hydrocarbon exploration (revised edition), *Geol. Surv. Isr., Rep. GSI/4/2008*, Israel.

Garfunkel, Z. (1981), Internal structure of the Dead Sea leaky transform (rift) in relation to plate kinematics, *Tectonophysics*, *80*(1–4), 81–108, doi:10.1016/0040-1951(81)90143-8.

Garfunkel, Z. (1998), Constrains on the origin and history of the eastern Mediterranean basin, *Tectonophysics*, *298*(1–3), 5–35, doi:10.1016/S0040-1951(98)00176-0.

Garfunkel, Z. (2014), Lateral motion and deformation along the Dead Sea transform, in *Dead Sea Transform Fault System: Reviews, Modern Approaches in Solid Earth Sciences*, vol. 6, edited by Z. Garfunkel et al., pp. 109–150, Springer, Dordrecht.

Garfunkel, Z., and Z. Ben-Avraham (1996), The structure of the Dead Sea basin, *Tectonophysics*, *266*(1–4), 155–176, doi:10.1016/S0040-1951(96)00188-6.

Genna, A., P. Nehlig, E. Le Goff, C. Guerrot, and M. Shanti (2002), Proterozoic tectonism of the Arabian Shield, *Precambrian Res.*, *117*(1–2), 21–40, doi:10.1016/S0301-9268(02)00061-X.

Guennoc, P., G. Pautot, M. Le Qentrec, and A. Coutelle (1990), Structure of an early oceanic rift in the northern Red Sea, *Oceanol. Acta*, *13*(2), 145–157.

Guiraud, R., and W. Bosworth (1999), Phanerozoic geodynamic evolution of northeastern Africa and the northwestern Arabian platform, *Tectonophysics*, *315*(1–4), 73–108, doi:10.1016/S0040-1951(99)00293-0.

Hansen, J. -A., S. G. Bergh, P. T. Osmundsen, and T. F. Redfield (2014), Stress inversion of heterogeneous fault-slip data with unknown slip sense: An objective function algorithm contouring method, *J. Struct. Geol.*, *70*, 119–140, doi:10.1016/j.jsg.2014.11.005.

Hardy, C., C. Homberg, Y. Eyal, E. Barrier, and C. Müller (2010), Tectonic evolution of the southern Levant margin since Mesozoic, *Tectonophysics*, *494*(3–4), 211–225, doi:10.1016/j.tecto.2010.09.007.

Hatzor, Y., and Z. Reches (1980), Structure and paleostresses in the Gilboa' region, western margins of the central Dead Sea rift, *Tectonophysics*, *180*(1), 87–100, doi:10.1016/0040-1951(90)90374-H.

Hawie, N. (2014), Architecture, geodynamic evolution and sedimentary filling of the levant basin: A 3D quantitative approach based on seismic data, PhD thesis, Earth Sciences, Univ. Pierre et Marie Curie, Paris, France.

Hempton, M. (1987), Constraints on Arabian plate motion and extensional history of the Red Sea, *Tectonics*, *6*(6), 687–705, doi:10.1029/TC006i006p00687.

Hippolyte, J. C., F. Bergerat, M. B. Gordon, O. Bellier, and N. Espurt (2012), Keys and pitfalls in mesoscale fault analysis and paleostress reconstructions, the use of Angelier's methods, *Tectonophysics*, *581*, 144–162, doi:10.1016/j.tecto.2012.01.012.

Homberg, C., and M. Bachmann (2010), Evolution of the Levant margin and western Arabian Platform since the Mesozoic: Introduction, in *Evolution of the Levant Margin and Western Arabia Platform Since the Mesozoic*, edited by C. Homberg et al., *Geol. Soc. London Spec. Publ.*, *341*, 1–8.

Homberg, C., E. Barrier, M. Mroueh, C. Müller, W. Hamdan, and F. Higazi (2010), Tectonic evolution of the central Levant margin (Lebanon) since Mesozoic, in *Evolution of the Levant Margin and Western Arabia Platform Since the Mesozoic*, edited by C. Homberg et al., *Geol. Soc. London Spec. Publ.*, *341*, 245–268.

Hu, J.-C., and J. Angelier (2004), Stress permutations: Three-dimensional distinct element analysis accounts for a common phenomenon in brittle tectonics, *J. Geophys. Res.*, *109*, B09403, doi:10.1029/2003JB002616.

Huibregtse, P., H. Alebeek, M. Zaal, and C. Biermann (1998), Palaeostress analysis of the northern Nijar and southern Vera basins: Constraints for the Neogene displacement history of major strike-slip faults in the Betic Cordilleras, SE Spain, *Tectonophysics*, *300*(1–4), 79–101, doi:10.1016/S0040-1951(98)00235-2.

Ibrahim, K. M., and W. J. McCourt (1995), Neoproterozoic granitic magmatism and tectonic evolution of the northern Arabian Shield: Evidence from Southwest Jordan, *J. Afr. Earth Sci.*, *20*(2), 103–118, doi:10.1016/0899-5362(95)00037-T.

Jarrar, G., R. J. Stern, G. Saffarini, and H. Al-Zubi (2003), Late- and post-orogenic Neoproterozoic intrusions of Jordan: Implications for crustal growth in the northernmost segment of the East African Orogen, *Precambrian Res.*, *123*(2–4), 295–319, doi:10.1016/S0301-9268(03)00073-1.

Joseph-Hai, N., Y. Eyal, and R. Weinberger (2010), Mesoscale folds and faults along a flank of a Syrian Arc monocline, discordant to the monocline trend, in *Evolution of the Levant Margin and Western Arabia Platform Since the Mesozoic*, edited by C. Homberg et al., *Geol. Soc. London Spec. Publ.*, *341*, 211–226.

Kaymakci, N., S. H. White, and P. M. Vandijk (2003), Kinematic and structural development of the Cankiri Basin (Central Anatolia, Turkey): A paleostress inversion study, *Tectonophysics*, *364*(1–2), 85–113, doi:10.1016/S0040-1951(03)00043-X.

Kazmin, V. G. (2002), *The Late Paleozoic to Cainozoic Intraplate Deformation in North Arabia: A Response to Plate Boundary Forces*, *EGU Stephan Mueller Spec. Publ. Ser.*, vol. 2, pp. 123–138, Copernicus Publications on behalf of the European Geosciences Union (EGU), Göttingen, Germany.
Kernstocková, M., and R. Melichar (2009), Numerical paleostress analysis the limits of automation, *Trab. Geol.*, *29*, 399–403.
Kolodner, K., D. Avigad, M. McWilliams, J. L. Wooden, T. Weissbrod, and S. Feinsten (2006), Provenance of north Gondwana Cambrian-Ordovician sandstone: U-Pb SHRIMP dating of detrital zircons from Israel and Jordan, *Geol. Mag.*, *143*(3), 367–391, doi:10.1017/S0016756805001640.
Küster, D. (2009), Granitoid-hosted Ta mineralization in the Arabian-Nubian Shield: Ore deposit types, tectono-metallogenetic setting and petrogenetic framework, *Ore Geol. Rev.*, *35*(1), 68–86, doi:10.1016/j.oregeorev.2008.09.008.
Lacombe, O. (2012), Do fault slip data inversions actually yield "paleostresses" that can be compared with contemporary stresses? A critical discussion, *C. R. Geosci.*, *344*(3–4), 159–173, doi:10.1016/j.crte.2012.01.006.
Lee, Y. J. (1991), Slickenside petrography: Slip-sense indicators and classification, MSc thesis, Dep. of Geol. Sc., State Univ. of New York at Albany, Albany.
Letouzey, J., and P. Tremolieres (1980), Paleo-stress fields around the Mediterranean since the Mesozoic from microtectonics: Comparison with plate tectonic data, *Rock Mech.*, *9*, 173–192.
Lowell, J. D., and G. J. Genik (1972), Sea-floor spreading and structural evolution of southern Red Sea, *Am. Assoc. Pet. Geol. Bull.*, *56*(2), 247–259.
Lyberis, N. (1988), Tectonic evolution of the Gulf of Suez and the Gulf of Aqaba, *Tectonophysics*, *153*(1–4), 209–220, doi:10.1016/0040-1951(88)90016-9.
Lyberis, N., T. Yurur, J. Chorowicz, E. Kasapoglu, and N. Gundogdu (1992), The East Anatolian Fault: An oblique collisional belt, *Tectonophysics*, *204*(1–2), 1–15, doi:10.1016/0040-1951(92)90265-8.
Matzenauer, E. (2012), Tectonics of the Préalpes Klippen and the Subalpine Molasse (Canton Fribourg, Switzerland), PhD thesis, Dep. of Geosci., Earth Sci., Univ. of Fribourg, Switzerland.
Mcclusky, S., et al. (2000), Global positioning system constraints on plate kinematics and dynamics in the eastern Mediterranean and Caucasus, *J. Geophys. Res.*, *105*(B3), 5695–5719, doi:10.1029/1999JB900351.
McQuarrie, N., J. M. Stock, C. Verdel, and B. P. Wernicke (2003), Cenozoic evolution of Neotethys and implications for the causes of plate motions, *Geophys. Res. Lett.*, *30*(20), 2036, doi:10.1029/2003GL017992.
Melichar, R., and M. Kernstockova (2010), 9D space—The best way to understand paleostress analysis, *Trab. Geol.*, *30*, 69–74.
Mikbel, S. H., and W. Zacher (1981), The Wadi Shueib structure in Jordan, *Neues Jahrb. Geol. Palaeontol., Monatsh.*, *9*, 571–576.
Moustafa, A. R. (1997), Controls on the development and evolution of transfer zones: The influence of basement structure and sedimentary thickness in the Suez rift and Red Sea, *J. Struct. Geol.*, *19*(6), 755–768, doi:10.1016/S0191-8141(97)00007-2.
Nemcok, M., and R. J. Lisle (1995), A stress inversion procedure for polyphase fault/slip data sets, *J. Struct. Geol.*, *17*(10), 1445–1453, doi:10.1016/0191-8141(95)00040-K.
Nemcok, M., D. Kovác, and R. J. Lisle (1999), A stress inversion procedure for polyphase calcite twin and fault/slip data sets, *J. Struct. Geol.*, *21*(6), 597–611, doi:10.1016/S0191-8141(99)00053-X.
Otsubo, M., K. Sato, and A. Yamaji (2006), Computerized identification of stress tensors determined from heterogeneous fault-slip data by combining the multiple inverse method and *k*-means clustering, *J. Struct. Geol.*, *28*(6), 991–997, doi:10.1016/j.jsg.2006.03.008.
Parlak, O., and M. Delaloye (1999), Precise $^{40}Ar/^{39}Ar$ ages from the metamorphic sole of the Mersin ophiolite (Southern Turkey), *Tectonophysics*, *301*(1–2), 145–158, doi:10.1016/S0040-1951(98)00222-4.
Pêcher, A., et al. (2008), Stress field evolution in the Northwest Himalayan syntaxis, Northern Pakistan, *Tectonics*, *27*, TC6005, doi:10.1029/2007TC002252.
Petit, J. P. (1987), Criteria for the sense of movement on fault surfaces in brittle rocks, *J. Struct. Geol.*, *9*(5–6), 597–608, doi:10.1016/0191-8141(87)90145-3.
Powell, J. H. (1989a), *Stratigraphy and Sedimentation of the Phanerozoic Rocks in Central and South Jordan, Part A: Ram and Khreim Groups*, *Geol. Direct., Geol. Map. Div. Bull.*, vol. 11, Natural Resources Authority, Amman, Jordan.
Powell, J. H. (1989b), *Stratigraphy and Sedimentology of the Phanerozoic Rocks in Central and South Jordan, Part B: Kurnub, Ajlun and Belqa Group*, *Geol. Direct., Geol. Map. Div. Bull.*, vol. 11, Natural Resources Authority, Amman, Jordan.
Powell, J. H., and B. K. Moh'd (2011), Evolution of Cretaceous to Eocene alluvial and carbonate platform sequences in central and south Jordan, *GeoArabia*, *16*(4), 29–82.
Rabb'a, I. (1994), *The Geology of the Al Qurayqira (Jabal Hamra Faddan) Map Sheet No. 3051 II*, *Geol. Direct., Geol. Map. Div. Bull.*, vol. 28, Natural Resources Authority, Amman, Jordan.
Radaideh, O. M. A., and R. Melichar (2014), A general comparison between the Paleostress methods, abstract paper presented at 12th Meeting of the Central European Tectonic Studies Group (CETeG), Lądek Zdrój, Poland, *Geologica Sudetica*, *42*, 77.
Rashdan, M. (1988), *The Regional Geology of Aqaba-Wadi Araba Area*, *sheets 3049-III*, *2949-II*, *Geol. Direct., Geol. Map. Div. Bull.*, vol. 7, Natural Resources Authority, Amman, Jordan.
Reiter, F., and P. Acs (2000), Tectonics FP demo-version 1.6. Software for Structural Geology, Kargl Computer & Consulting, Rüsselsheim, Germany.
Robertson, A. H. F. (1998), Mesozoic–Tertiary tectonic evolution of the easternmost Mediterranean area: Integration of marine and land evidence, in *Proceedings of the Ocean Drilling Program*, *Sci. Results*, vol. 160, edited by A. H. F. Robertson et al., pp. 723–782, Ocean Drilling Program, Texas A&M Univ., Tex.
Rothwell Group, L. P. (2011), PaleoWeb v.1.1, plate-tectonics modelling software for ArcGIS Desktop™, User's Guide, Houston, Tex.
Saintot, A., and J. Angelier (2000), Plio-Quaternary paleostress regimes and relation to structural development in the Kertch-Taman peninsulas (Ukraine and Russia), *J. Struct. Geol.*, *22*(8), 1049–1064, doi:10.1016/S0191-8141(00)00025-0.
Saintot, A., and J. Angelier (2002), Tectonic paleostress fields and structural evolution of the NW-Caucasus fold-and-thrust belt from Late Cretaceous to Quaternary, *Tectonophysics*, *357*(1–4), 1–31, doi:10.1016/S0040-1951(02)00360-8.
Saintot, A., M. B. Stephens, G. Viola, and Ø. Nordgulen (2011), Brittle tectonic evolution and paleostress field reconstruction in the southwestern part of the Fennoscandian Shield, Forsmark, Sweden, *Tectonics*, *30*, TC4002, doi:10.1029/2010TC002781.
Salameh, E., and W. Zacher (1982), Horizontal stylolites and paleostress in Jordan, *Neues Jahrb. Geol. Palaeontol.*, *8*, 509–512.
Schattner, U., Z. Ben Avraham, M. Reshef, G. Bar-Am, and M. Lazar (2006), Oligocene-Miocene formation of the Haifa basin: Qishon-Sirhan rifting coeval with the Red Sea-Suez rift system, *Tectonophysics*, *419*(1–4), 1–12, doi:10.1016/j.tecto.2006.03.009.
Segev, A. (1984), Lithostratigraphy and paleogeography of the marine Cambrian sequence in southern Israel and southwestern Jordan, *Isr. J. Earth Sci.*, *33*, 26–33.

Sengor, A. M. C., and Y. Yilmaz (1981), Tethyan evolution of Turkey: A plate tectonic approach, *Tectonophysics*, *75*(3–4), 181–241, doi:10.1016/0040-1951(81)90275-4.
Shahar, J. (1994), The Syrian arc system: An overview, *Palaeogeogr. Palaeoclimatol. Palaeoecol.*, *112*(1–2), 125–142.
Shan, Y., Z. Li, and G. Lin (2004), A stress inversion procedure for automatic recognition of polyphase fault/slip data sets, *J. Struct. Geol.*, *26*(5), 919–925, doi:10.1016/j.jsg.2003.10.001.
Sharland, P. R., R. Archer, D. M. Casey, R. B. Davies, S. H. Hall, A. P. Heward, A. D. Horbury, and M. D. Simmons (2001), *Arabian Plate Sequence Stratigraphy*, *GeoArabia Spec. Publ.*, vol. 2, Gulf PetroLink, Manama, Bahrain.
Sippel, J., M. Scheck-Wenderoth, K. Reicherter, and S. Mazur (2009), Paleostress states at the south-western margin of the Central European Basin System—Application of fault-slip analysis to unravel a polyphase deformation pattern, *Tectonophysics*, *470*(1–2), 129–146, doi:10.1016/j.tecto.2008.04.010.
Smit, J., J.-P. Brun, S. Cloetingh, and Z. Ben-Avraham (2010), The rift-like structure and asymmetry of the Dead Sea Fault, *Earth Planet. Sci. Lett.*, *290*(1–2), 74–82, doi:10.1016/j.epsl.2009.11.060.
Sperner, B., and P. Zweigel (2010), A plea for more caution in fault–slip analysis, *Tectonophysics*, *482*(1–4), 29–41, doi:10.1016/j.tecto.2009.07.019.
Sperner, B., L. Ratschbacher, and R. Ott (1993), Fault-striae analysis: A Turbo Pascal program package for graphical presentation and reduced stress tensor calculation, *Comput. Geosci.*, *19*(9), 1361–1388, doi:10.1016/0098-3004(93)90035-4.
Stern, R. J. (1994), Arc-assembly and continental collision in the Neoproterozoic East African Orogen: Implications for the consolidation of Gondwanaland, *Annu. Rev. Earth Planet. Sci.*, *22*, 319–351, doi:10.1146/annurev.ea.22.050194.001535.
Stesky, R. M., and G. W. Pearce (1995), *Spheristat 2.2 for Windows*, Pangaea Scientific, Brockville, Ont., Canada.
Stockli, R., E. Vermote, N. Saleous, R. Simmon, and D. Herring (2005), The Blue Marble Next Generation—A true color earth dataset including seasonal dynamics from MODIS, Dataset User's manual, NASA Earth Observatory.
Stoeser, D. B., and C. D. Frost (2006), Nd, Pb, Sr, and O isotopic characterization of Saudi Arabian Shield terranes, *Chem. Geol.*, *226*(3–4), 163–188, doi:10.1016/j.chemgeo.2005.09.019.
Taymaz, T., J. Jackson, and D. McKenzie (1991), Active tectonics of the North and Central Aegean Sea, *Geophys. J. Int.*, *106*(2), 433–490, doi:10.1111/j.1365-246X.1991.tb03906.x.
Thisse, Y., P. Guennoc, G. Poult, and Z. Nawab (1983), The Red Sea: A natural geodynamic and metallogenic laboratory, *Episodes*, *3*, 3–8.
Tripathy, V., and D. Saha (2013), Plate margin paleostress variations and intracontinental deformations in the evolution of the Cuddapah basin through Proterozoic, *Precambrian Res.*, *235*, 107–130, doi:10.1016/j.precamres.2013.06.005.
Vail, J. R. (1983), Pan-African crustal accretion in northeast Africa, *J. Afr. Earth Sci.*, *1*(3–4), 285–294, doi:10.1016/S0731-7247(83)80013-5.
Walker, J. D., J. W. Geissman, S. A. Bowring, and L. E. Babcock (Comps.) (2012), *Geologic Time Scale v. 4.0*, Geol. Soc. of Am., Colo., doi:10.1130/2012.CTS004R3C.
Wallace, R. E. (1951), Geometry of shearing stress and relation to faulting, *J. Geol.*, *59*(2), 118–130, doi:10.1086/625831.
Walley, C. D. (1998), Some outstanding issues in the geology of Lebanon and their importance in the tectonic evolution of the Levantine region, *Tectonophysics*, *298*, 37–62, doi:10.1016/S0040-1951(98)00177-2.
Wdowinski, S., and E. Zilberman (1997), Systematic analyses of the large-scale topography and structure across the Dead Sea Rift, *Tectonics*, *16*(3), 409–424, doi:10.1029/97TC00814.
Yamaji, A. (2000), The multiple inverse method: A new technique to separate stresses from heterogeneous fault-slip data, *J. Struct. Geol.*, *22*(4), 441–452, doi:10.1016/S0191-8141(99)00163-7.
Yamaji, A., K. Sato, and M. Otsubo (2005), Multiple Inverse Method Software Package, Main Processor version 5.31, User's Guide, Div. of Earth and Planet. Sci., Kyoto Univ., Japan.
Yamaji, A., M. Otsubo, and K. Sato (2006), Paleostress analysis using the Hough transform for separating stresses from heterogeneous fault-slip data, *J. Struct. Geol.*, *28*(6), 980–990, doi:10.1016/j.jsg.2006.03.016.
Yamaji, A., K. Sato, and M. Otsubo (2011), Multiple Inverse Method Software Package, Main Processor version 6.2, User's Guide, Div. of Earth and Planet. Sci., Kyoto Univ., Japan.
Zain-Eldeen, U., D. Delvaux, and P. Jacobs (2002), *Tectonic Evolution in the Wadi Araba Segment of the Dead Sea Rift, South-West Jordan*, *EGU Stephan Mueller Spec. Publ. Ser.*, vol. 2, pp. 63–81, Copernicus Publications on behalf of the European Geosciences Union (EGU), Göttingen, Germany.
Žalohar, J. (2009), T-TECTO 3.0 Professional. Integrated software for structural analysis of fault-slip data, Dep. of Geol., Univ. of Ljubljana, Ljubljana, Slovenia.
Žalohar, J., and M. Vrabec (2007), Paleostress analysis of heterogeneous fault slip data: The Gauss method, *J. Struct. Geol.*, *29*(11), 1798–1810, doi:10.1016/j.jsg.2007.06.009.
Zanchi, A., G. B. Crosta, and A. N. Darkal (2002), Paleostress analyses in NW Syria: Constraints on the Cenozoic evolution of the northwestern margin of the Arabian plate, *Tectonophysics*, *357*(1–4), 255–278, doi:10.1016/S0040-1951(02)00371-2.
Ziegler, M. A. (2001), Late Permian to Holocene paleofacies evolution of the Arabian Plate and its hydrocarbon occurrences, *GeoArabia*, *6*(3), 445–504.